Anode break excitation in rat and guinea pig ventricular cardiomyocytes

Summary

Excitation at the closure of the anode is one of the two ways to electrically elicit action potentials in single cells. Despite the fact that “anode break” excitation has long observed in cardiac myocytes (the phenomenon of anodal excitation of cardiac muscle has been described by Cranefield et al., in the late-1950s; later also Dekker demonstrated that the myocardium could be excited by anodal stimuli), very little is known about its mechanism and implications. Understanding the mechanism and properties of anodal stimulation has been an area of active research for decades. Anodal stimulation has been implicated in improved cardiac output with pacing and the potentially arrhythmogenic “supernormal excitability”. Characterizing the fundamental basis of anodal stimulation will advance the understanding of excitability in the heart and the mechanism of these clinically important features of anodal excitation in the ventricular myocardium.

Using the patch clamp whole-cell technique, we challenged single rat and guinea pig ventricular myocytes with hyperpolarizing current pulses in order to estimate the success rate of anode break excitation in the two species. We measured and compared strength-duration curves for cathodal and anodal stimulations in rat and guinea pig myocytes and found that the ratio between anodal and cathodal rheobase was much higher in guinea pig than in rat. We also found that maximum rate of depolarization (dV/dt_{max}) increased during anode break as compared with cathodal stimulation and did more so in rat than in guinea pig. When hyperpolarizing current pulses were consecutively delivered at a fixed duration and very close to the current threshold for excitation, action potentials were elicited at variable delays after anode break. We finally measured strength-interval curves to investigate cathodal and anodal excitability in diastole and during refractory period and found supernormal anodal excitability during the repolarization phase of rat action potentials. We demonstrated, for the first

time, that supernormal excitability of the refractory heart to anode break excitation has its source at the cellular level.

In the section “state of the art” of this appendix I will analyze the work of Ranjan et al. (“Mechanism of anode break stimulation in the heart”, Biophys. J., 1998) which demonstrates, for the first time, that anode break excitation has an active cellular basis. In fact Ranjan et al. recorded in single isolated ventricular cells from a variety of mammalian species action potentials anodally induced verifying that anodal stimulation could arise exclusively from active cardiac tissue properties and found that the activation of a hyperpolarization-activated inward current (I_f) provided the current necessary to drive the potential to more depolarized levels, and the time-dependent block of inwardly rectifying K^+ current (I_{K1}) aided the process by increasing membrane resistance. These findings provided a cellularly based rationale for anode break stimulation.

In the section “materials and methods” I will explain protocols for obtain “strength-duration” and “strength-interval” curves for cathodal and anodal stimulations. In the section “results and discussion” I will present and briefly discuss the results reported above. Finally in the section “conclusions and future developments” I will discuss the possibility to use the anodal stimulation in a pacemaker programmed to bipolar pacing configuration where heart is paced both with the cathode and anode electrodes.

State of the art

Tissue based explanation of anodal stimulation

The heart can be stimulated by either cathodal and anodal stimulation (Cranefield et al., 1957; Dekker, 1970). Cathodal stimulation of the heart or any other excitable tissue is explained by stimulating electrode injecting current in the tissue underneath it, causing direct depolarization of the cells in the region (Hoffman and Cranefield, 1960). Anodal current injection results in hyperpolarization of the underlying tissue (Brooks et al., 1955; Cranefield et al., 1957), so that the ability to trigger an action potential is paradoxical. So how does one explain the routinely observed anodal stimulation of the heart? Anodal stimulation can occur during the stimulus pulse (make stimulation) or upon the termination of the pulse (break stimulation) (Dekker, 1970). Anodal stimulation of cardiac tissue has been explained using bidomain models of cardiac tissue (Henriquez, 1993). Bidomain models postulate different electrical anisotropies in the intracellular and interstitial domains of the heart (Henriquez et al., 1990). Bidomain models predict that the unequal anisotropy in the two domains will lead to marked inhomogeneties membrane potential in nearby tissue (Roth and Wikswo, 1994). During anodal stimulation, a "dog bone"-shaped region of the tissue underlying the stimulating electrode becomes hyperpolarized, whereas regions lying in the convexity of the dog bone become depolarized and are referred to as "virtual cathodes" (Roth, 1992). It is proposed that, during anodal stimulation, the excitation wavefront starts from these virtual cathodes (Wikswo, 1994). Anodal stimulation at the onset of the stimulating pulse (anode make stimulation) can be explained by this model. For anode break stimulation, the bidomain model assumes that a steady state has been reached during the anodal pulse with regions of hyperpolarized and depolarized tissue; upon termination of the stimulus pulse, excitation propagates from the hyperpolarized tissue region as a result of depolarization extending from the virtual cathodes (Roth, 1995; Wikswo et al., 1995) (figure 1).

Membrane currents at hyperpolarized potentials

A hyperpolarization-activated current was identified in normal (Yu et al., 1995; Cerbai et al., 1996) and failing (Cerbai et al., 1994, 1997) ventricular myocytes. Except for its voltage dependence, this current appears to be identical to the I_f described in Purkinje fibers and in nodal cells. Another current whose properties change with hyperpolarization is the inward rectifier, I_{K1}. At hyperpolarized potentials the current carried by I_{K1} channels is blocked in a time-dependent manner (Carmeliet, 1980; Mitra and Morad, 1991). If the unblocking of this channel at depolarized potentials is time-dependent as well, it could play a significant role in bringing about anodal stimulation.

Hypothesis

If anodal stimulation can be elicited in isolated cell preparations, no passive tissue properties could be involved. Anodal stimulation would then have to have an active basis. If active mechanisms suffice to produce anodal stimulation, isolated ventricular cells should manifest excitability in response to anodal stimulation. Isolated cell preparations eliminate the passive network tissue properties that have been postulated to underline anodal excitation in multicellular preparations.

Cellular explanation of Anode break excitation

Rajan et al. performed current clamp experiments on isolated mammalian cardiac myocytes to test the hypothesis that active membrane properties are involved in anodal excitation. Action potentials were recorded upon the break of anodal stimulation. Representative action potentials induced in canine and rat ventricular cells, recorded under current clamp conditions by Ranjan et al. with anodal stimulation, are shown in figure 2. Ranjan et al. observed Anode break responses in guinea pig, rat and canine ventricular myocytes. Thus anode break excitation exists in single isolated ventricular cells from a variety of mammalian species, demonstrating that such excitation need not depend upon passive tissue properties. To understand the ionic basis of anodal stimulation, Ranjan et al. measured membrane currents in isolated mammalian ventricular cells at increasingly negative potentials. I_{K1} is the predominant current at hyperpolarized potentials. Figure 3 shows the membrane currents activated by hyperpolarization, beginning with a transient spike of capacity current. Thereafter, at

−160 mV, there is an instantaneous activation of I_{K1} that is subsequently gets blocked in a time-dependent manner. At a more hyperpolarized potential (−200 mV), the decay of I_{K1} is much faster, and there is activation of another inward current, the hyperpolarization-activated current, I_f. To dissect the two current components that change with hyperpolarization, Ranjan et al. used different ionic conditions and voltage clamp protocols. I_{K1} was studied at hyperpolarized potentials under physiological ionic conditions. Because the activation and blocking of I_{K1} current are much faster than the reported activation time constant of I_f (Yu et al., 1995), all of the I_{K1}-related recordings were made before there was any significant activation of I_f. To isolate I_f, Ranjan et al. used barium to block I_{K1}. To quantify the block of I_{K1} at negative potentials and its subsequent unblock at voltages near the resting potential, Ranjan et al. performed voltage clamp experiments. As reported earlier, the block was found to be time- and voltage-dependent, becoming faster and more pronounced as the potential became more negative (Biermans et al., 1989). The block of I_{K1} during a hyperpolarizing pulse is clearly time-dependent. If the unblocking is time-dependent as well, then the magnitude of I_{K1} will be reduced just after the potential is stepped back to more depolarized levels. This reduction in I_{K1} after the termination of the pulse will facilitate depolarization beyond the resting potential. To test if the unblocking of I_{K1} is indeed time-dependent, Ranjan et al. held the cell at −80 mV, stepped to −150 mV until steady-state block was reached, and then stepped back to more depolarized potentials. Figure 4A shows that, after Ranjan et al. stepped back to less negative voltages, there was a time-dependent increase in current as the channels unblocked. The growing current (shown in figure 4B) is inward or outward, depending on whether the pulse is positive or negative with respect to the equilibrium potential for potassium ions (E_K). Both the block and the unblock of the current could be well-fit with single exponentials. The time constants at various potentials for block (*circles*) and unblock (*squares*) are shown in Fig. 4*C*. To quantify the hyperpolarization-activated inward current (I_f), Ranjan et al. used 8mM external barium to block I_{K1}. Figure 5 shows the membrane current elicited by hyperpolarization in canine (A), guinea pig (B) and rat (C). A slowly activating inward current is observed. The time constant of activation is similar to that of I_f (Yu et al., 1995). Figure 5 also shows the slowly decaying tail currents. Ranjan et al. determined the voltage dependence of activation of the channel (Figure 5*D*) by measuring instantaneous tail currents. The time constant of activation was found to be longer in

canine and guinea pig than in rat cells, in agreement with published results for I_f (Yu et al., 1995; Cerbai et al., 1996). As is evident from Figure 5*D*, the current is activated at more negative potentials in canine and guinea pig than in rat cells. Even though the current is activated at potentials below normal physiological potentials (particularly in canine and guinea pig cells), these potentials are well within the range that is predicted to be achieved in tissue beneath a stimulating electrode (Roth, 1995). For anodal stimulation, it would be more relevant to the anodal pacing literature (e.g., Furman et al., 1989) to examine the currents activated as a result of short hyperpolarizing pulses. If the current activated during the hyperpolarizing pulse results in persistent inward tail current, it can provide the inward current needed to depolarize the cell to the threshold of sodium current activation. To test whether any inward tail current is activated as a result of hyperpolarizing pulses of short duration, Ranjan et al. recorded current in cells held at varying hyperpolarizing potentials for 15 ms and then stepped to a test potential of −80 mV. Figure 6 shows representative currents recorded from a rat myocyte. At the more hyperpolarized potentials, an inward current activates during the pulse, with corresponding inward tail currents when the cell is stepped back to −80 mV. The deactivation time constant of the current at −80 mV is large, similar to that of I_f (Yu et al., 1995). The presence of I_f is critical at potentials ranging from the resting potential to the threshold for sodium current, as it may provide the inward current needed to depolarize the membrane and trigger an action potential. Thus Ranjan et al. quantified I_f at these potentials. Fig. 7*A* shows the tail current amplitudes measured at −70 and −90 mV in dog, guinea pig, and rat myocytes after holding the cells at −150 mV for 2 s. Then Ranjan et al. modified the action potential model developed by Luo and Rudy to include I_f as well as the time-dependent blocking and unblocking of I_{K1}. The modeling results confirmed that these current densities suffice to initiate anode break excitation. In fact simulations performed to test for anodal excitation, using the unmodified model, showed that anodal stimulation produced hyperpolarization of the cell, which returned monotonically to the resting potential upon the release of the pulse. Simulation performed with the modified model exhibited anode break stimulation. Figure 8 (A and B) shows the results of simulations using the unmodified model and (C and D) the modified model. Fig. 9 shows the currents that are active during a stimulating pulse), and in the interval preceding the anode break action potential. Upon the break of the pulse, I_f remains inward and drives the potential to more depolarized levels until the

threshold for activation of the sodium current is reached and the upstroke occurs. To gauge the relative importance of I_f and I_{K1} in the process of anode break stimulation, Ranjan et al performed simulations with action potential models that 1) included I_f but no I_{K1} block, 2) had no I_f but included I_{K1} block, and 3) included both I_f and I_{K1} block. Figure 10 shows the results of current clamp simulations run for the same stimulus strength and duration for the three cases. In Fig. 10 *a*, with no I_{K1} block present in the model, anode break stimulation is not observed at this stimulus strength, even though the deactivating I_f does drive the transmembrane potential above the resting level. The slight decrease in the magnitude of I_{K1} observed toward the end of the current clamp pulse is because of activation of inward I_f, which drives the membrane potential to more depolarized levels, reducing the driving force for I_{K1}. For higher stimulus strengths, anode break stimulation could be observed when enough I_f was activated to drive the potential to the threshold for activation of the sodium current. In Figure 10*b*, with no I_f present in the model, no anode break stimulation could be generated. With the time-dependent reduction of I_{K1} conductance during the stimulus pulse, the cell is hyperpolarized to a greater extent than in Fig 10 *a*, even though the stimulus strength remains the same. Nevertheless, with no I_f present in the model, there is no net inward current to drive the transmembrane potential above the resting level, and hence no anode break stimulation can occur. This was the case even with very strong hyperpolarizations. In Fig. 10 *c*, with both I_f and I_{K1} block present, anode break stimulation is faithfully reproduced.

It appears clear from this study that active membrane properties play a significant role in the process of anodal stimulation. The activation of I_f provides the current necessary to drive the potential to more depolarized levels, and the time-dependent block of I_{K1} aids the process by increasing membrane resistance.

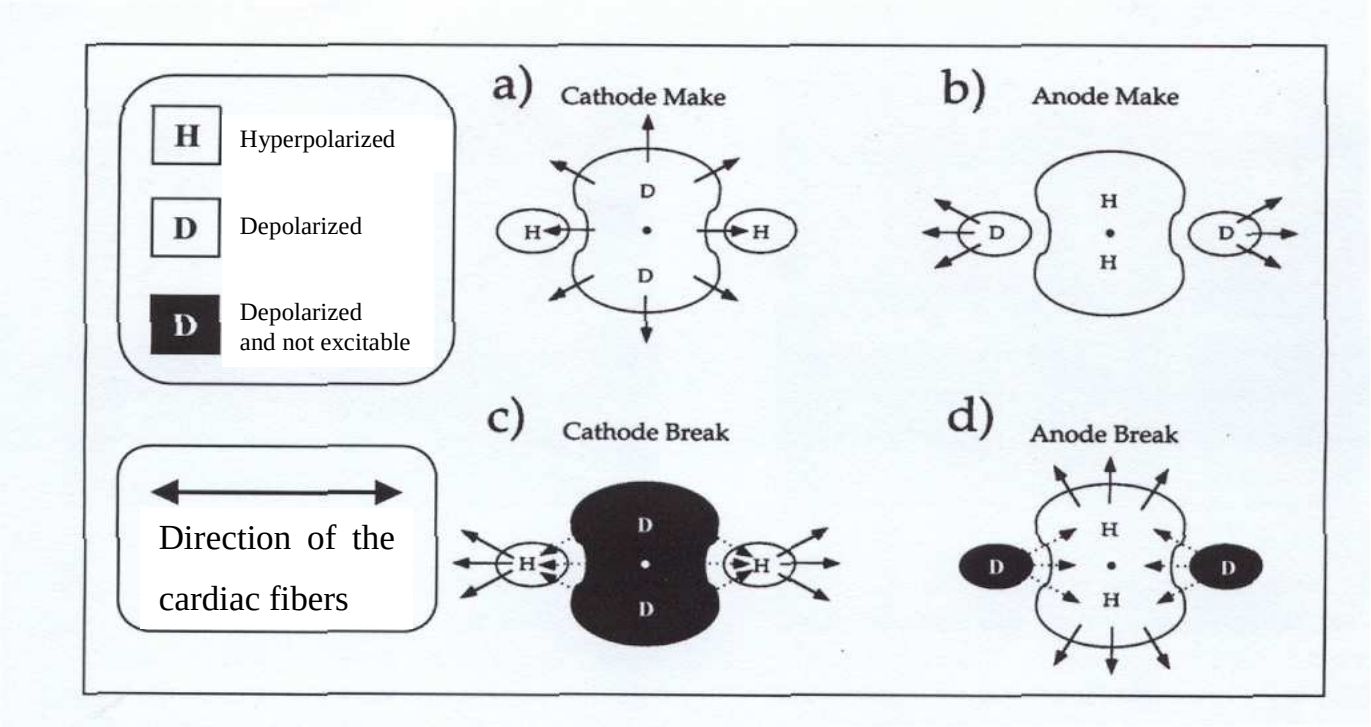

Fig 1 The "dog bone" distribution of transmembrane potential in response to cathodal and anodal stimulations. *For anodal stimulations (b and d), the region in the immediate vicinity of the stimulating electrode is hyperpolarized (marked by an H in the figures). In response to anodal stimulation "virtual cathodes" are set up along the fiber in the convexity of hyperpolarized region, slightly away from the stimulating electrode where the tissue is depolarized (marked by D in the figure). (Modified from Roth, 1996).*

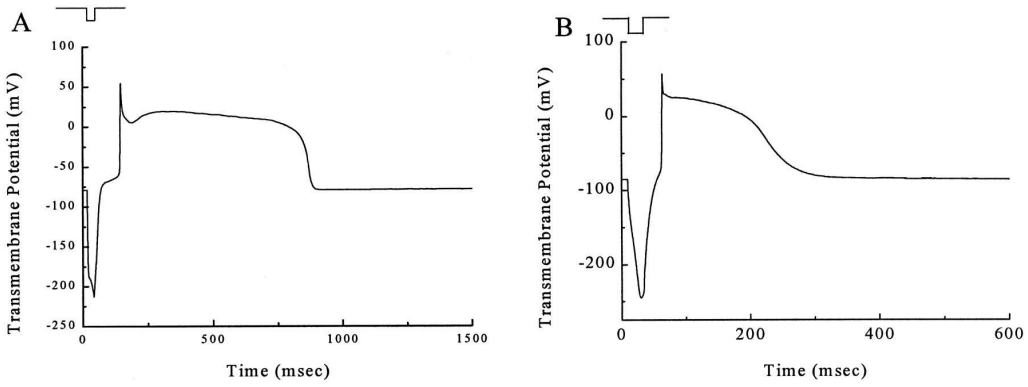

Figure 2. Action potentials induced by anodal stimulation in (A) canine and (B) rat ventricular myocytes. *The time for which the stimulus was applied to the cells is indicated by the bar on top of the figures. A 50-ms pulse was applied to the canine cell and a 20-ms pulse to the rat cell.*

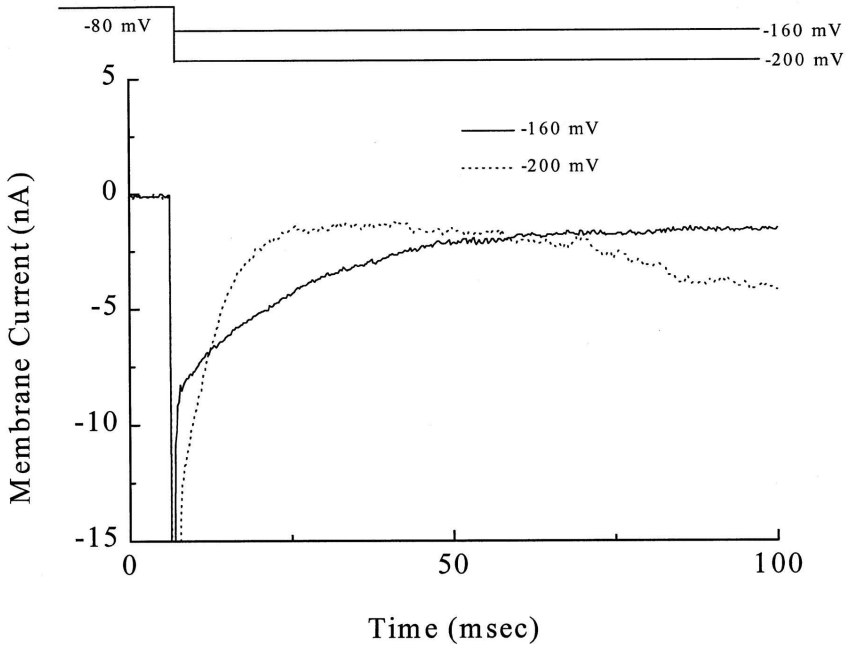

Figure 3. Total ionic current in response to hyperpolarizing voltage clamp steps in a canine myocyte under normal physiological ionic conditions. *At −160 mV there is a time-dependent blocking of the current carried by the I_{K1} channels. At −200 mV the blocking of I_{K1} is faster, and an inward current (I_β) is activated.*

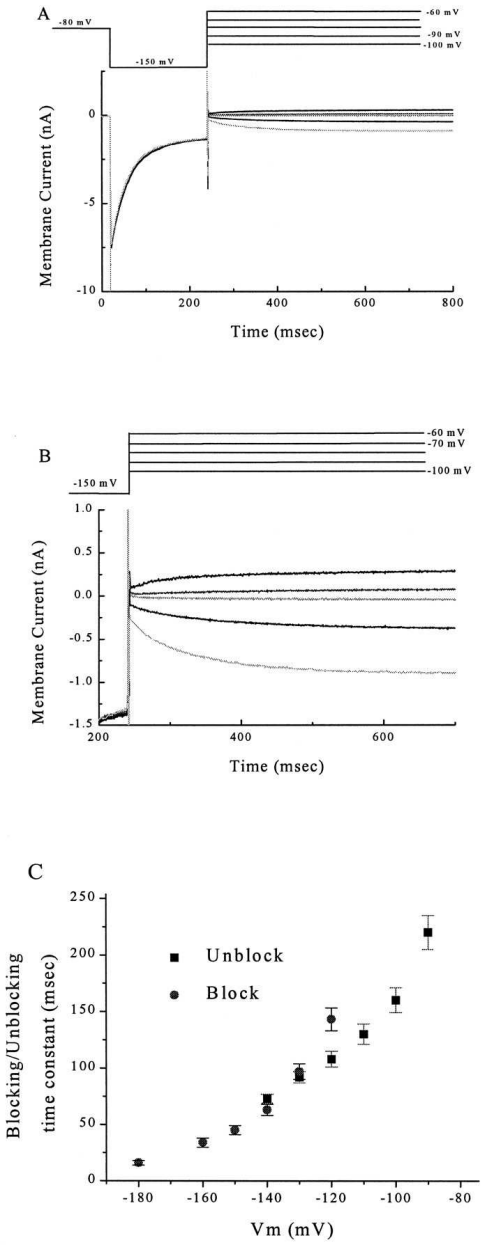

Figure 4. Time-dependent unblocking of I_{K1}. *(A) Current recorded from a rat myocyte held at a hyperpolarizing voltage to induce block and then stepped to a more depolarized tail potential to demonstrate time-dependent unblock of I_{K1}. (B) Same as A, with an expanded scale to illustrate the unblocking. There is an increase in current with time, and the direction of the current is dependent on whether the pulse is positive or negative to E_K. (C) Time constant of I_{K1} block/unblock (n = 5).*

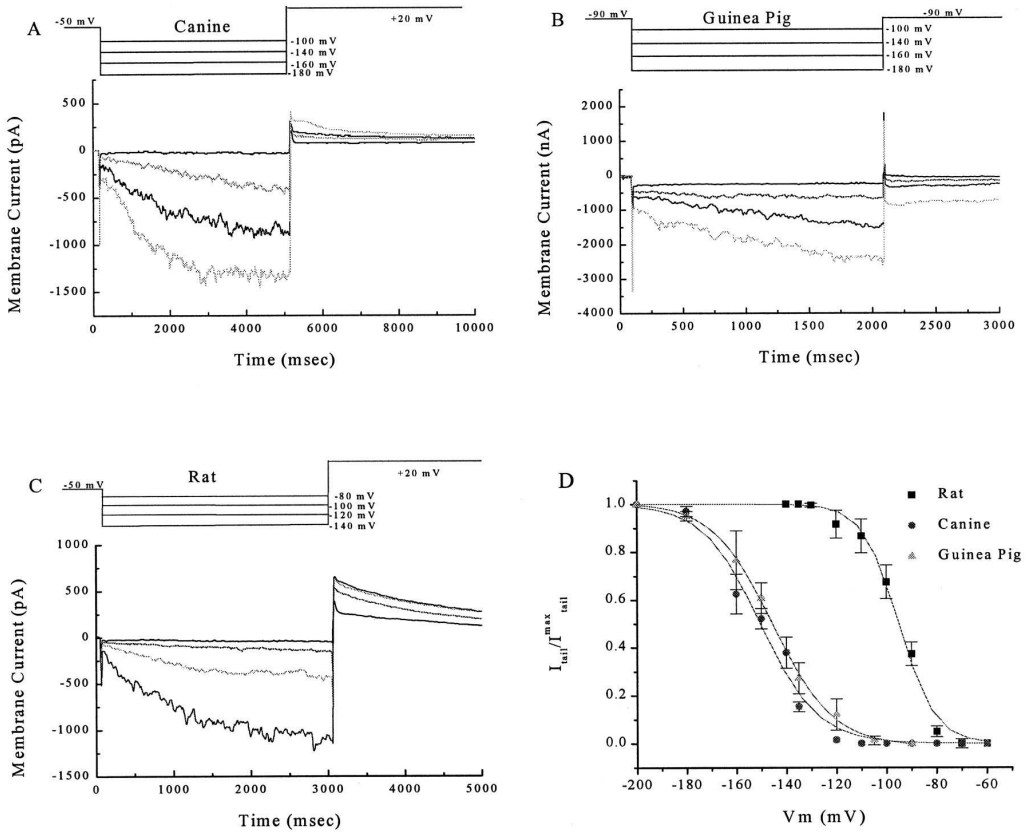

Figure 5. I_f in ventricular myocytes. *The recordings were made in the presence of 8 mM Ba^{2+} in the bath solution to block I_{K1}. (A-C) Representative currents in canine (A), guinea pig (B), and rat (C) ventricular myocyte. (D) The activation curve for canine, guinea pig, and rat cells determined from the tail current after different hyperpolarizing pulses activating the current. Data points represent mean ± SD (n = 5, n = 4 for guinea pig cells). Solid lines represent a sigmoidal fit to the data using the Boltzman equation. $V_{1/2}$ = −150 mV for canine cells, −145 mV for guinea pig cells, and −93.9 mV for rats cells with a slope factor of 12.2 mV for canine, 12.0 for guinea pig, and 7.4 mV for rat cells.*

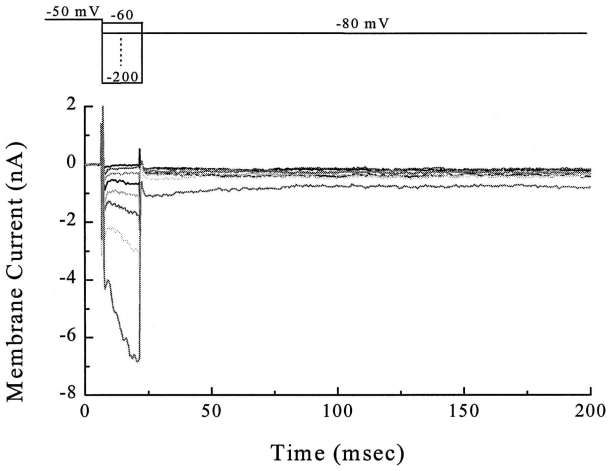

Figure 6. Inward current activated by short hyperpolarizing pulses in a rat ventricular myocyte. *Short hyperpolarizing pulses of 15 ms were delivered before switching to a test potential of −80 mV. At hyperpolarized potentials an inward current is recorded. The current is larger and the activation more rapid at more negative potentials.*

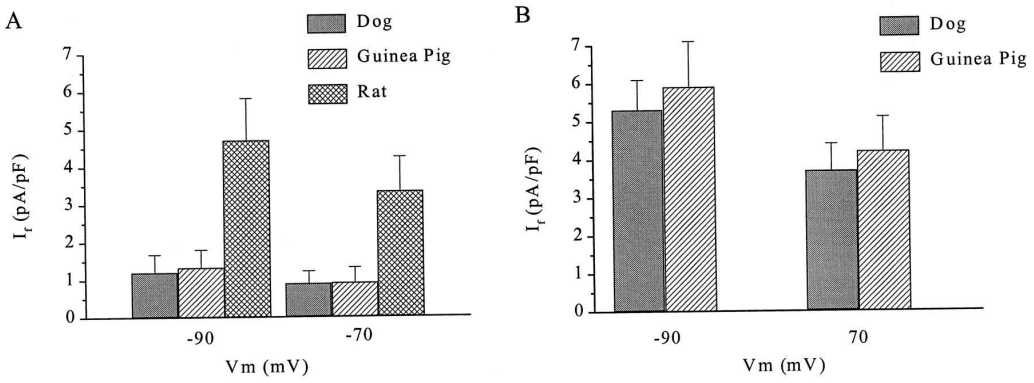

Figure 7. I_f tail currents in dog, guinea pig, and rat cells. *(A) The myocytes were held at −150 mV for 2 s, and then the tail current was measured at a test potential of −70 and −90 mV (n = 5 for dog and rat, n = 4 for guinea pig). (B) The cell was held at −180 mV for 2 s, and the current was measured at test potentials of −70 and −90 mV.*

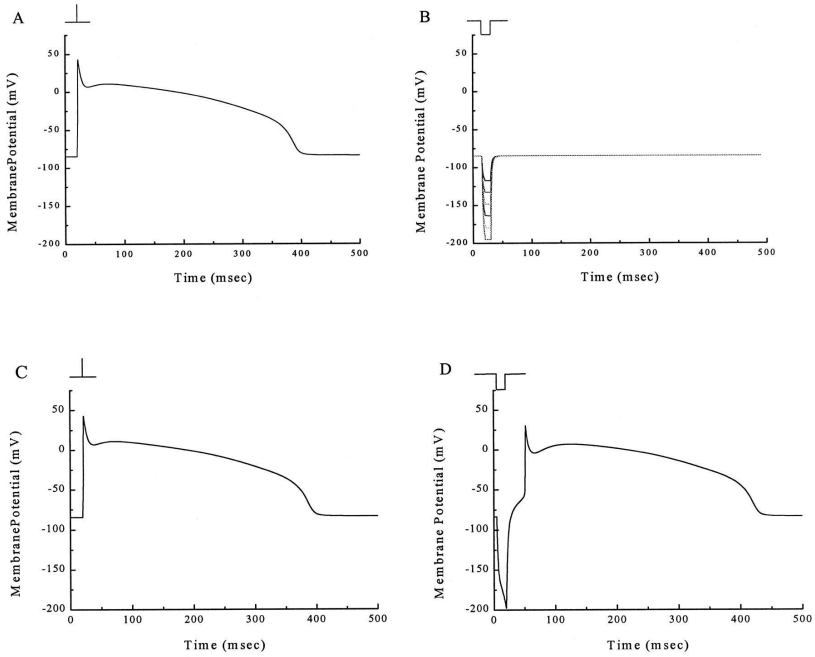

Figure 8. Action potential model. *(A and B) Results of simulations using the unmodified Luo-Rudy model for cathodal and anodal stimulation, respectively. Anodal stimulation results in hyperpolarization of the cell, which returns to normal resting potential at the termination of the pulse. The bar at the top of the figures indicates the application of the stimulus pulse. For cathodal stimulation a 2-ms pulse was applied, and for anodal stimulation a 15-ms pulse was applied. (C and D) Result of simulations using the modified Luo-Rudy model for cathodal and anodal stimulation, respectively. The response of the modified model to cathodal stimulation is the same as that of the unmodified model. In response to anodal stimulation, the modified model exhibits anode break stimulation.*

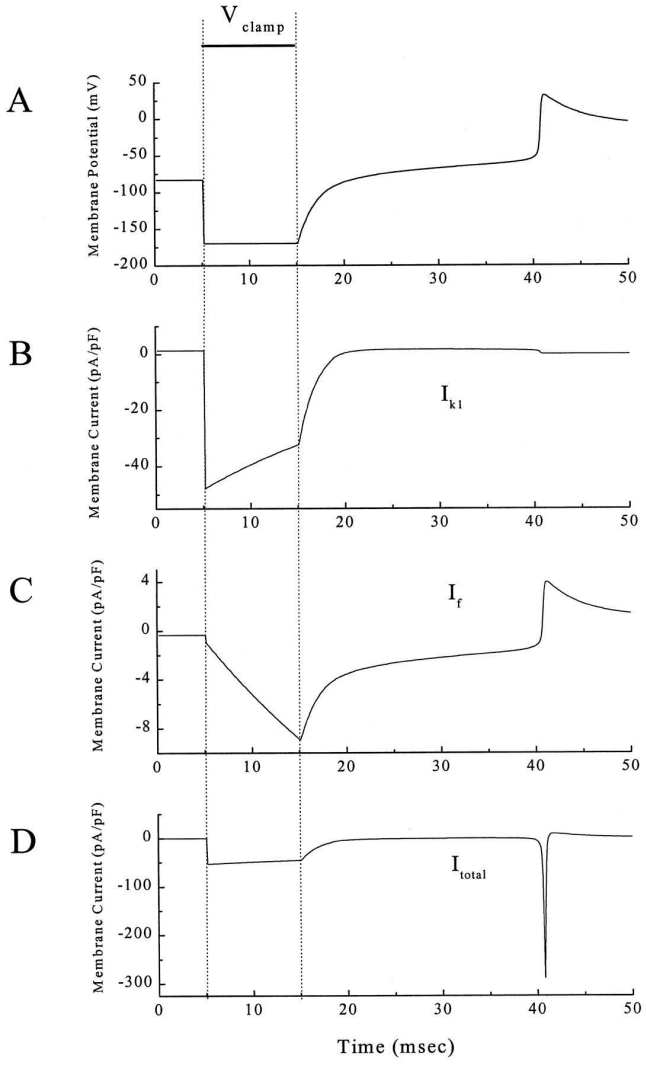

Figure 9. The role of different currents in the generation of anodal stimulation. *The modified Luo-Rudy model was used for those simulations in which the cell was clamped at −170 mV for 10 ms (indicated by the vertical dotted lines). (A) The transmembrane potential. (B) The inward rectifier I_{K1} current. Note the reduction in current with time during the voltage clamp pulse. (C) Hyperpolarization-activated I_f current. The current is activated by the hyperpolarizing pulse and is inward until the action potential upstroke occurs, providing the current needed to drive the transmembrane potential to the threshold of activation for the sodium current. (D) Total current. The large inward current is the sodium current coinciding with the action potential upstroke.*

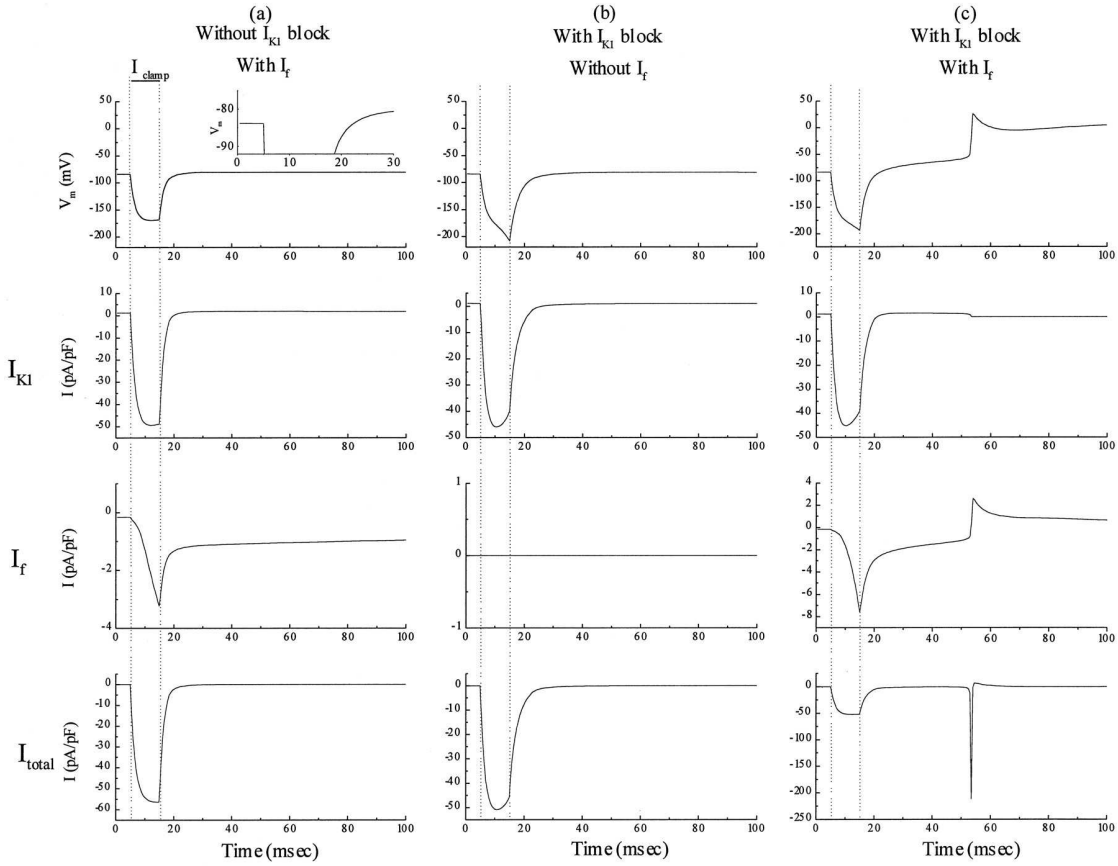

Figure 10. Result of simulations done with the models, with (a) time-independent I_{K1} and I_f; (b) time-dependent I_{K1} and no I_f; and (c) time-dependent I_{K1} and I_f. *The results of model a are shown in the first column with the transmembrane potential in row 1, I_{K1} in row 2, I_f in row 3, and I_{total} in row 4. All of the current clamp simulations in this figure are of the same stimulus strength. Model a) did not elicit an anode break response at this stimulus strength. I_f was activated during the pulse and provided the inward current to drive the membrane potential above the resting potential (shown in the inset on an expanded scale), but was not enough to elicit an action potential. Results of model b) are shown in column 2. There is a reduction of I_{K1} current during the stimulus pulse, even though the driving force is increasing, simulating the block of the channel. Model c) (column 3) exhibits an anode break response for this stimulus strength.*

Materials and methods

Cell isolation

Single cells were enzymatically isolated from adult male Wistar rat and guinea pig left ventricles. Each rat and guinea pig was anaesthetized with ether inhalation and killed by decapitation. The heart was rapidly removed, mounted on a Langendorff apparatus, and perfused at 37°C with the following sequence of solutions: Ca^{2+}-free (control, no added calcium) Tyrode solution for 5 min to remove the blood, low-Ca^{2+} (0.1mm) solution containing 1mg ml^{-1} type 2 collagenase (Worthington, Lakewood, NJ, USA) and 0.1 mg ml^{-1} type XIV protease (Sigma Aldrich, Milan, Italy) for 20 min, and enzyme-free low-Ca^{2+} solution for 5 min. The left ventricle was then minced and shaken for 10 min in the low-Ca^{2+} solution. Myocytes were stored at room temperature in the control solution with 0.5mM Ca^{2+}. All experiments were performed within 2–8 h after isolation. The procedure was approved by the Veterinary Animal Care and Use Committee of the University of Parma and conformed to the National Ethical Guidelines (Italian Ministry of Health; D.L.vo 116, January 27, 1992).

Solutions

Isolation solution contained (mm): 126 NaCl, 22 dextrose, 5.0 $MgCl_2$, 4.4 KCl, 20 taurine, 5 creatine, 5 sodium pyruvate, 1 NaH_2PO_4 and 24 Hepes (pH adjusted to 7.4 with NaOH). The solution was gassed with 100% O_2. Normal Tyrode solution (NT) for bathing of cells during experiments contained the following (mM): 126 NaCl, 11 dextrose, 5.4 KCl, 1.0 $MgCl_2$, 1.08 $CaCl_2$ and 24 Hepes (pH adjusted to 7.4 with NaOH). The pipette filling solution contained (mm): 113 KCl, 10 NaCl, 5.5 dextrose, 5 K_2ATP, 0.5 $MgCl_2$ and 10 Hepes (pH adjusted to 7.1 with KOH). A drop of storage solution containing cells was placed in the experimental chamber (~2.5 ml) and superfused by gravity at a flow rate of about 2 ml min^{-1}. The temperature of the solutions in the cell bath was 37°C.

Electrical recordings

Suction pipettes were made from borosilicate capillary tubing (Harvard Apparatus, Eden bridge, UK) and had a resistance, when filled, of 2–4 MΩ. Transmembrane potential (V_m) was recorded by means of an Axoclamp 2B amplifier (Axon Instruments, Union City, CA, USA), adopting the whole-cell configuration of the patch clamp technique. Transmembrane potential was digitized at a sampling frequency of 20 kHz for "strength-duration" protocols and 5 kHz for "strength-interval" protocols with a 12-bit analog-to-digital converter (Digidata 1200 Series Interface, Axon Instruments). Before a cell was contacted with the pipette tip, the pipette potential was set to zero and the voltage drop across the pipette was compensated with the bridge balance. Resting potential of the cells was about ~72 mV. In strength-duration current clamp protocols single cardiomyocytes from rat and guinea pig left ventricles were stimulated, at a frequency of 1 Hz, with current pulses having variable intensity and duration which were regulated by an external stimulator (Crescent Instruments). At the beginning the duration of the stimulus was set up to 1 ms and the current was manually increased in 0.2 nA steps until an action potential was elicited. The duration of the stimulus was progressively increased in 1 ms steps until 10 ms. For each duration a threshold current was measured. For anodal "strength-duration" protocol the external stimulator was set up to inject hyperpolaring current pulses. For cathodal "strength-duration" protocol depolarizing current pulses were injected (anodal and cathodal "strength-duration" protocols figure 1).

In "strength-interval" current clamp protocols each single rat cardiomyocyte was stimulated with a train of five constant depolarizing current pulses (3 ms, 2–3 nA), at a frequency of 1 Hz, in the way to elicit five conditioning action potentials. The last conditioning pulse (S1) was followed by a premature pulse (S2) having a variable intensity and interval (S1-S2) as regards the last conditioning action potential. S2 pulses of 3 ms for both anodal and cathodal strength-interval protocols were examined. To test the threshold current of S2 trough the diastolic period, the S1-S2 interval was decremented in 25 ms steps beginning at 275-325 ms. When approaching refractoriness, the testing interval was progressively shortened in 10 to 5 ms steps until S2 no longer elicited an action potential in response to currents as large as 20 nA. To measure the threshold current, S2 pulse was progressively increased in amplitude in 0.2 nA steps for each examined S1-S2 interval. For anodal strength-interval protocol the external

stimulator was set up to inject hyperpolaring S2 pulses. For cathodal strength-interval protocol depolarizing S2 pulses were inejcted (anodal and cathodal “strength-interavl” protocols figure 2, 3, 4, 5).

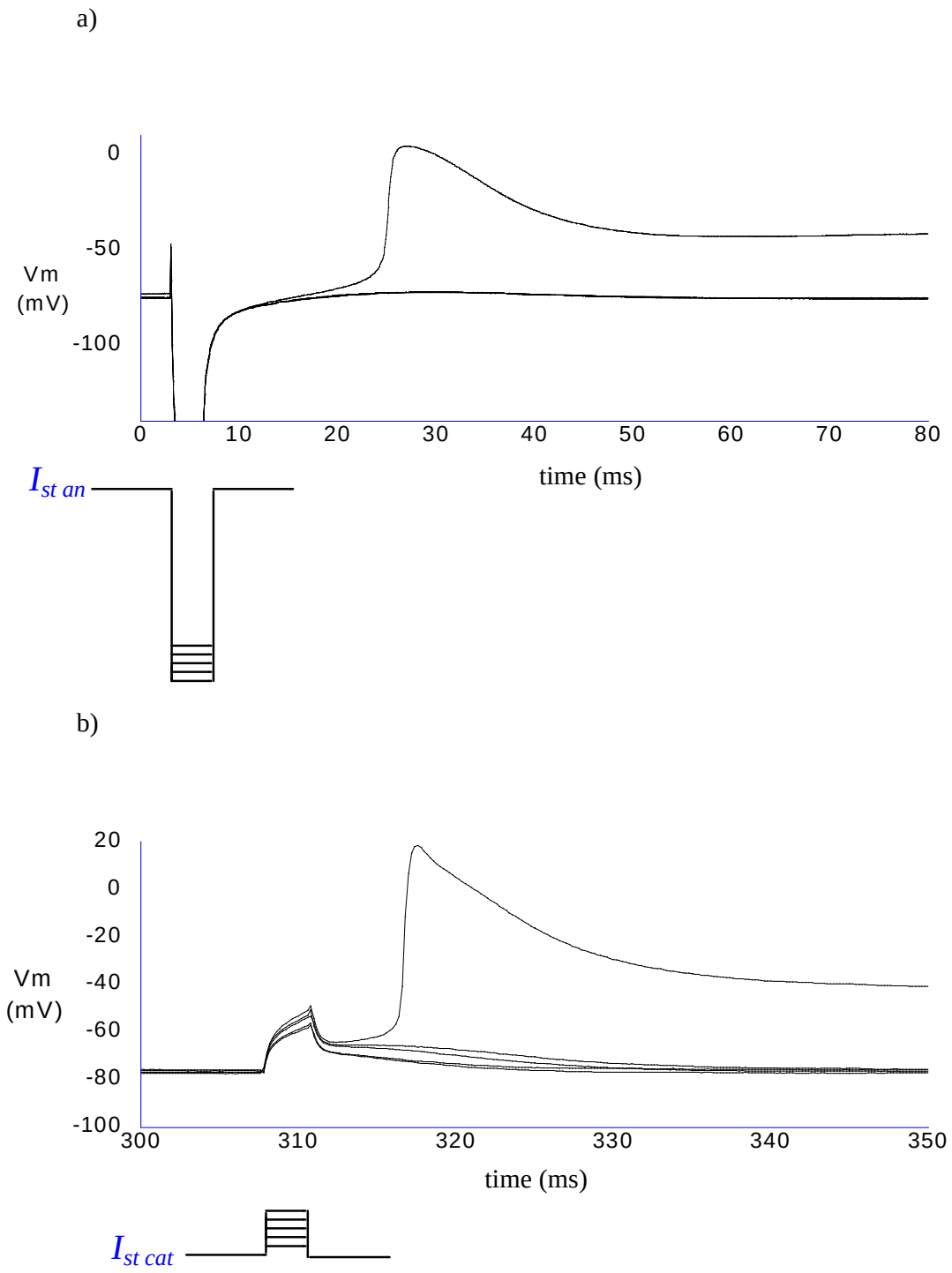

Figure 1. Example of anodal (a) and cathodal (b) strength-duration current clamp protocol*. Current pulses of 3 ms were increased in 0.2 nA steps until action potential was elicited . Threshold current was -17.72 nA in (a) and 1.41 nA in (b).*

Anodal stimulation (S2) in the diastolic period

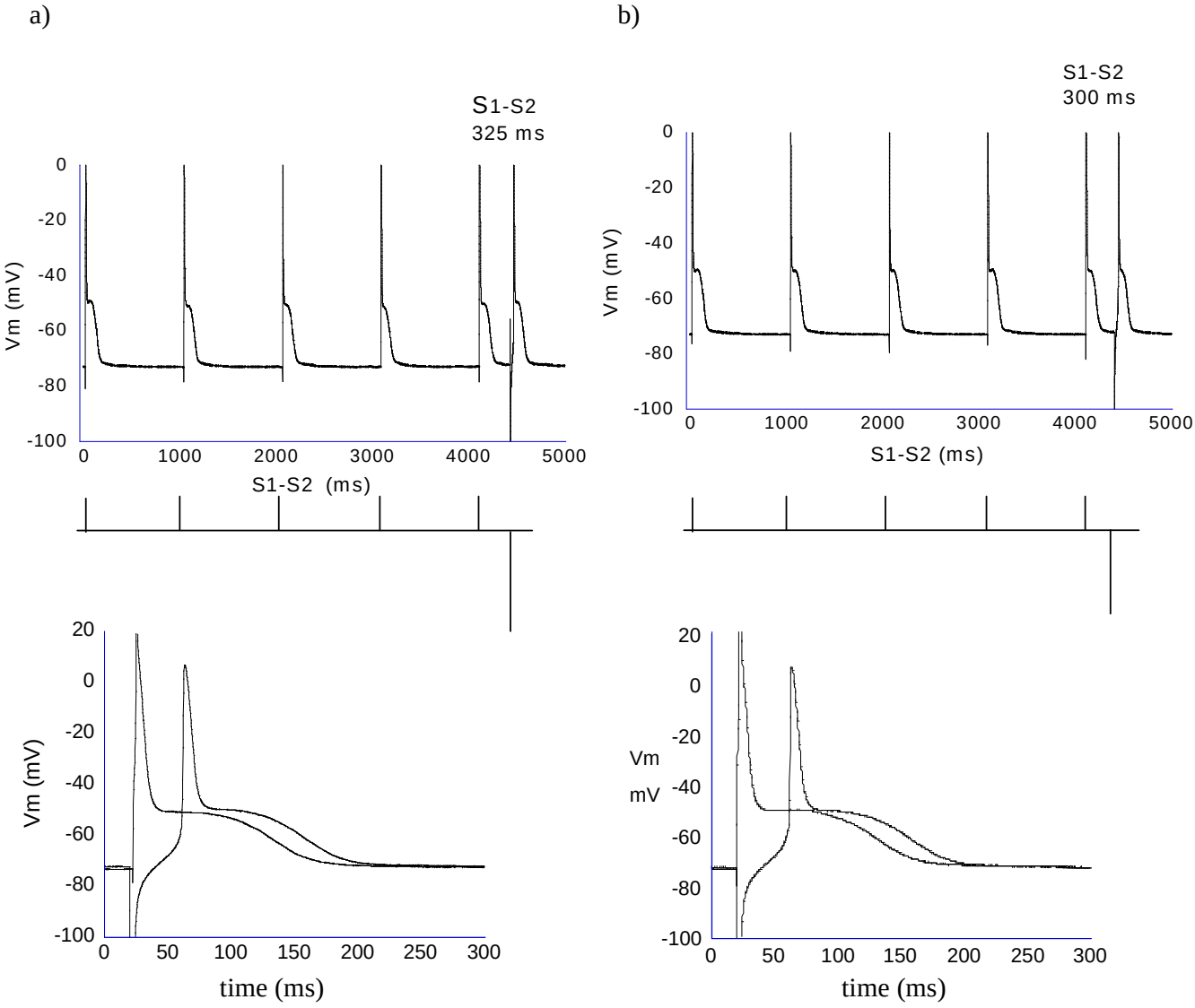

Figure 2. Example of anodal strength-interval current clamp protocol in the diastolic period. *To test the anodal threshold current of S2 trough the diastolic period, the S1-S2 interval was decremented in 25 ms steps beginning at 325 ms. Threshold current of S2 was -8.66 nA at S1-S2 of 325 ms (a) and -8.15 nA at S1-S2 of 300 in (b). In insets the last conditioning action potential and the anodal action potential are superimposed in order to have the same onset.*

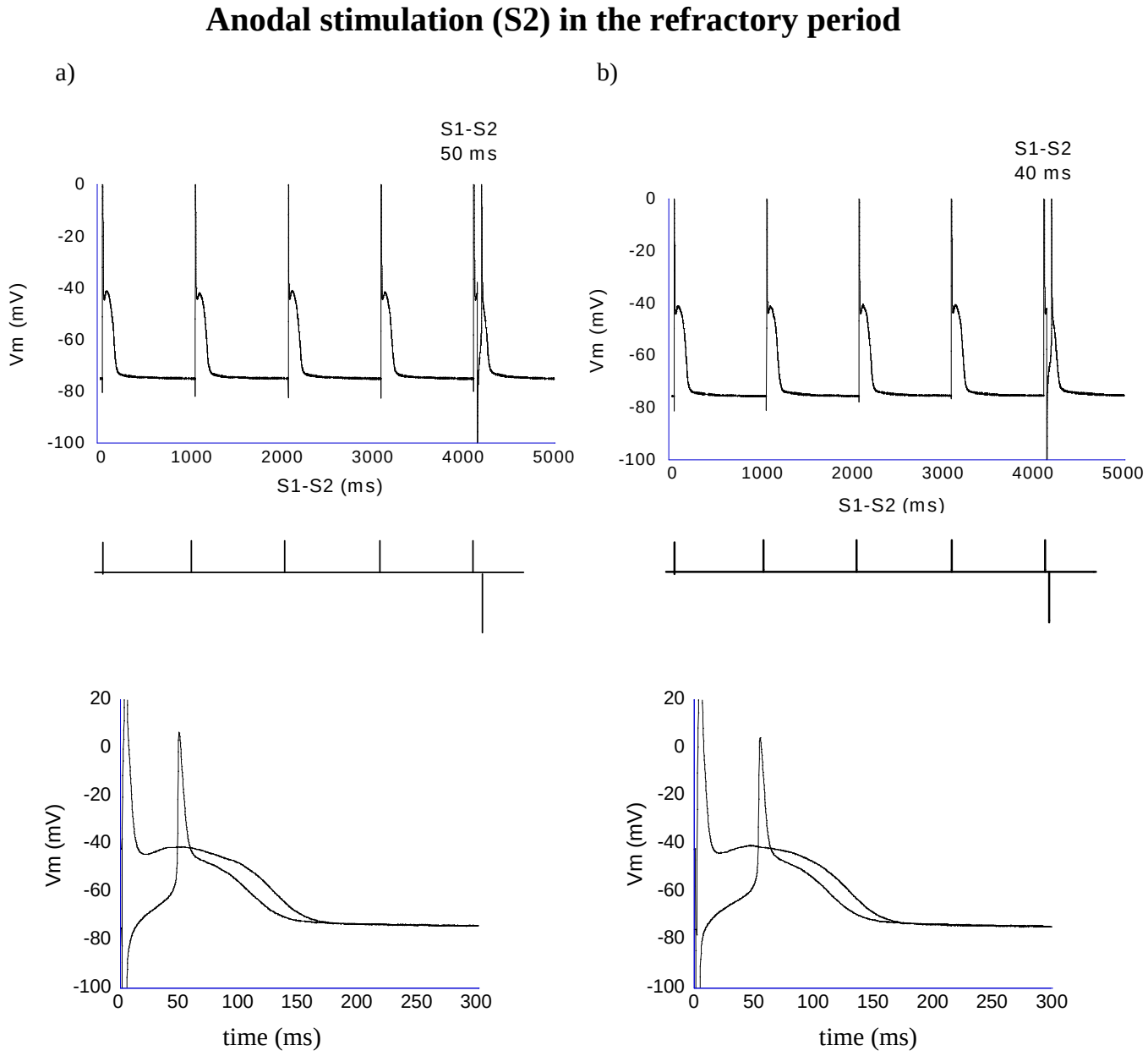

Figure 3. Example of anodal strength-interval current clamp protocol in the refractory period. *To test the anodal threshold current of S2 trough the refractory period, the S1-S2 interval was decremented in 10 ms steps beginning at 50 ms. Threshold current of S2 was -5.54 nA at S1-S2 of 50 ms (a) and -4.64 nA at S1-S2 of 40 in (b). In insets the last conditioning action potential and the anodal action potential are superimposed in order to have the same onset.*

Cathodal stimulation (S2) in the diastolic period

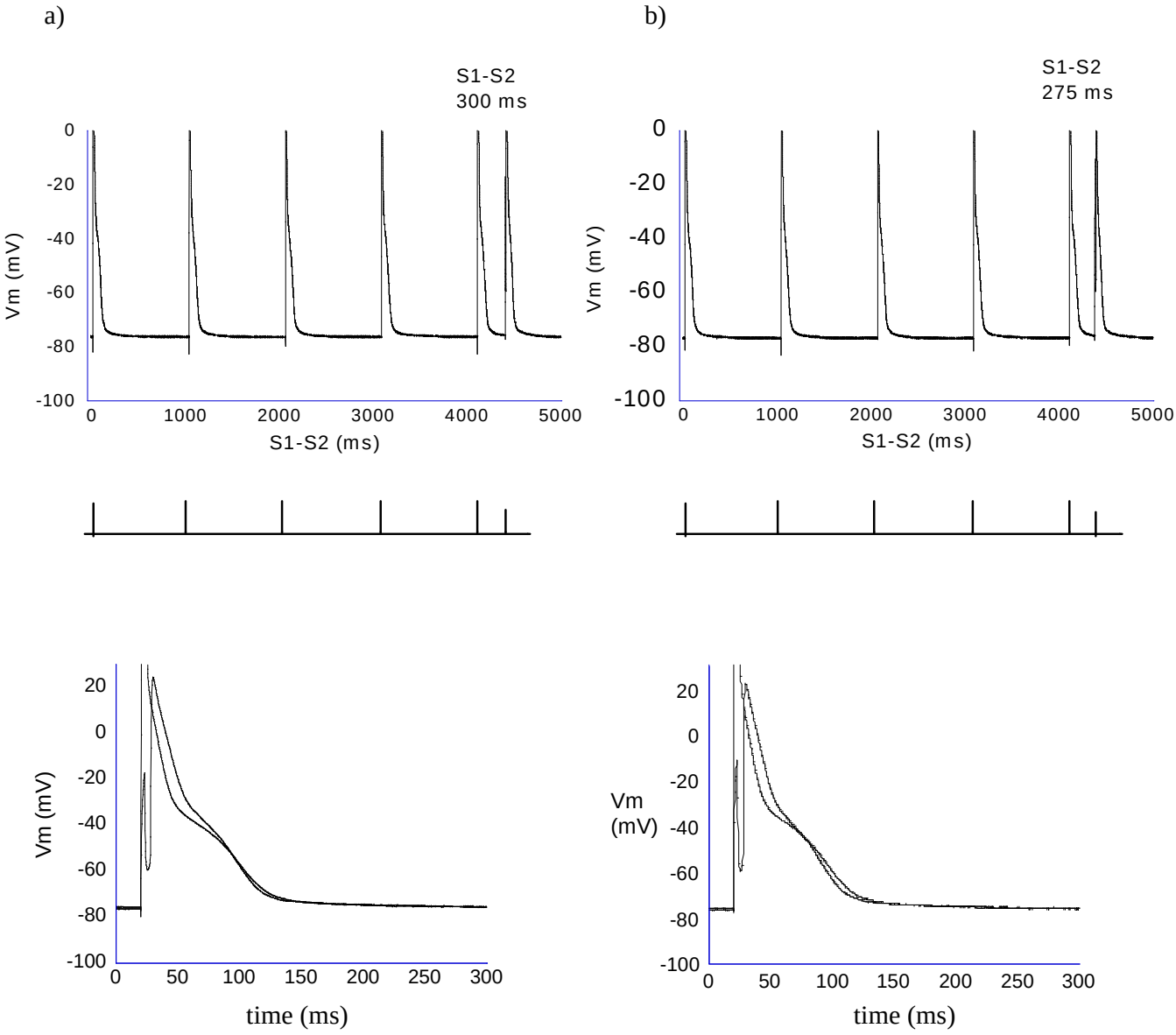

Figure 4. Example of cathodal strength-interval current clamp protocol in the diastolic period. *To test the cathodal threshold current of S2 trough the diastolic period, the S1-S2 interval was decremented in 25 ms steps beginning at 300 ms. Threshold current of S2 was 1.5 nA at S1-S2 of 300 ms (a) and 1.42 nA at S1-S2 of 275 in (b). In insets the last conditioning action potential and the cathodal action potential are superimposed in order to have the same onset.*

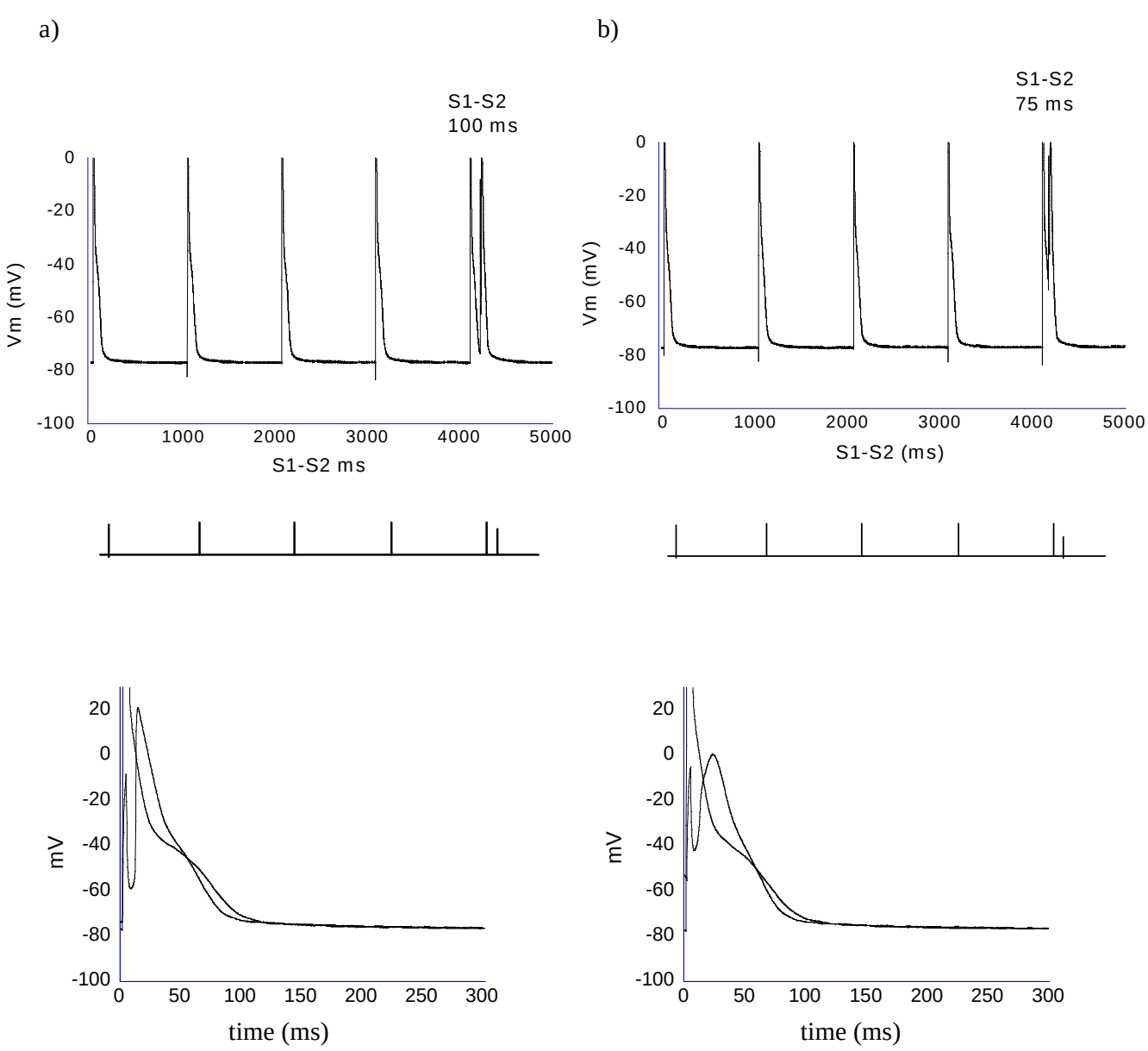

Figure 5. Example of cathodal strength-interval current clamp protocol in the refractody period. *To test the cathodal threshold current of S2 trough the refractory period, the S1-S2 interval was decremented in 25 ms steps beginning at 100 ms. Threshold current of S2 was 1.5 nA at S1-S2 of 100 ms (a) and 1.05 nA at S1-S2 of 75 in (b). In insets the last conditioning action potential and the cathodal action potential are superimposed in order to have the same onset.*

Results and discussion

Anode break excitation in guinea pig and rat ventricular cardiomyocytes

We performed current clamp experiments on isolated rat and guinea pig left ventricular cardiomyocytes in order to test the hypothesis of Ranjan et al. that active membrane properties are involved in anodal excitation. Figure 1 shows representative action potentials induced in rat (a) and guinea pig (b) ventricular myocytes under current clamp conditions with anodal stimulation. During the current injection itself, the membrane simply hyperpolarized, but after termination of the stimulus the membrane potential reached the sodium current threshold and an action potential ensued. Thus anode break excitation existed in the single ventricular cells that we tested. In accord with Ranjan et al., we verified that anode break excitation need not depend upon passive tissue properties. In particular, we challenged 12 guinea pig and 47 rat myocytes with 1-200 ms for guinea pig and 1-10 ms for rat and 0-20 nA hyperpolarizing current pulses in order to estimate the success rate of anode break in the two species. We found that 39 rat (82.9%) and 7 guinea pig (58.3%) cells exhibited anode break excitation. We believe that this different is due to a different density of I_{K1} in the two species: the time-independent, inwardly rectifying K^+ current (I_{K1}) strongly modulates the resting membrane potential. The mean membrane resistence (R_m) in rat at resting potential that we measured was $R_{m\ rat}$ = 37 MΩ and the mean capatitance (C_m) was $C_{m\ rat}$ = 160 pF. By these results it was possible to measure an estimate of the I_{K1} density in rat: $d_{Ik1\ rat}$ = 169 pS / pF. We did same measures on published mean values of R_m and C_m in guinea pig (R_m = 32 MΩ e C_m = 72 pF, Hume and Uehara, 1985) and we obtained a value of $d_{Ik1\ guinea\ pig}$ = 430 pS / pF. In fact, for stimuli of the same strength and duration, the likelihood of eliciting an anodal action potential in rat was higher than guinea pig cadiomyocytes due to a lower I_{K1} density (figure 2).

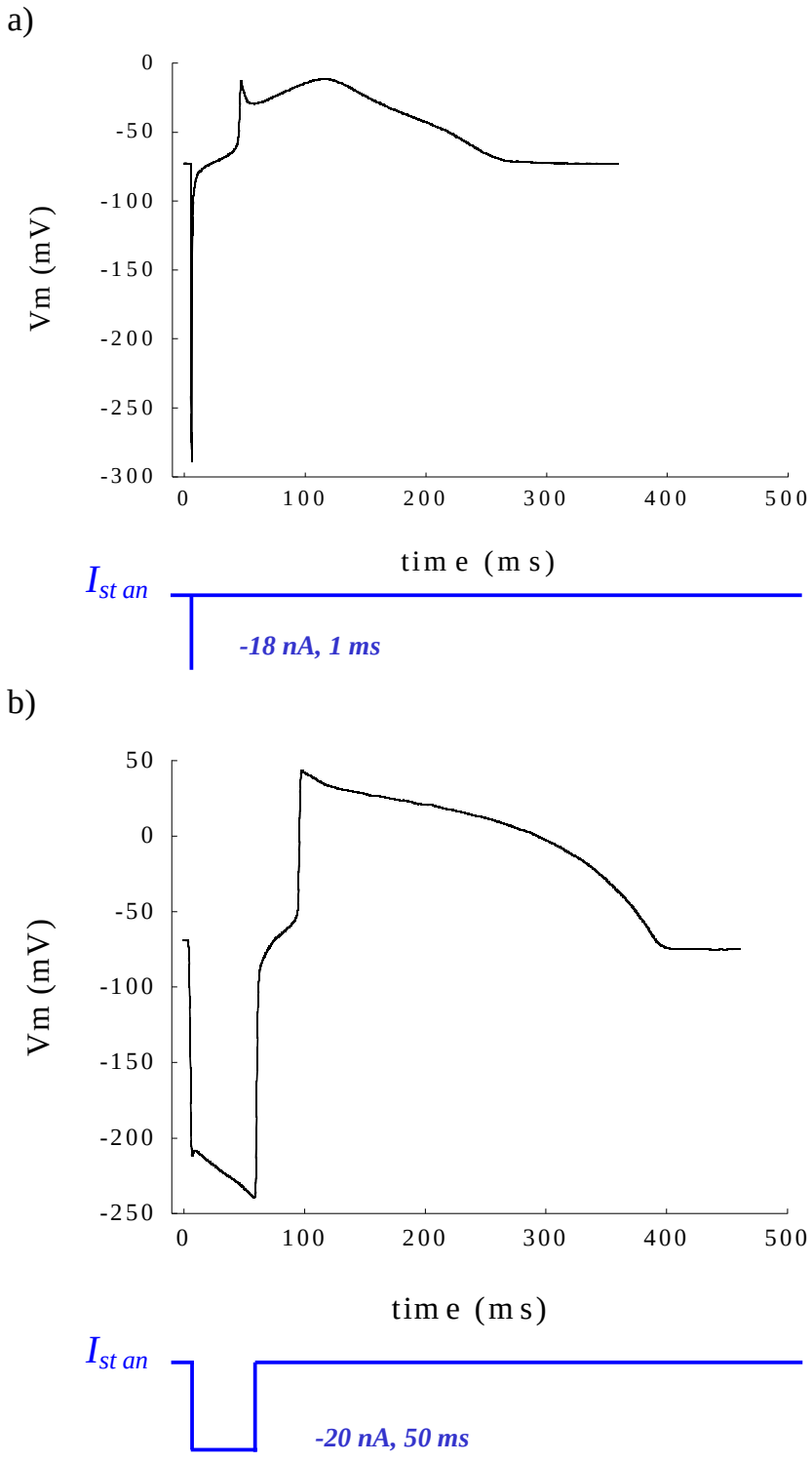

Figure 1. Representative action potentials induced by anodal stimulation in a) rat and b) guinea pig left ventricular cardiomyocytes. *The times and durations for which the stimuli were applied to the cells are indicated by the bars under the figures.*

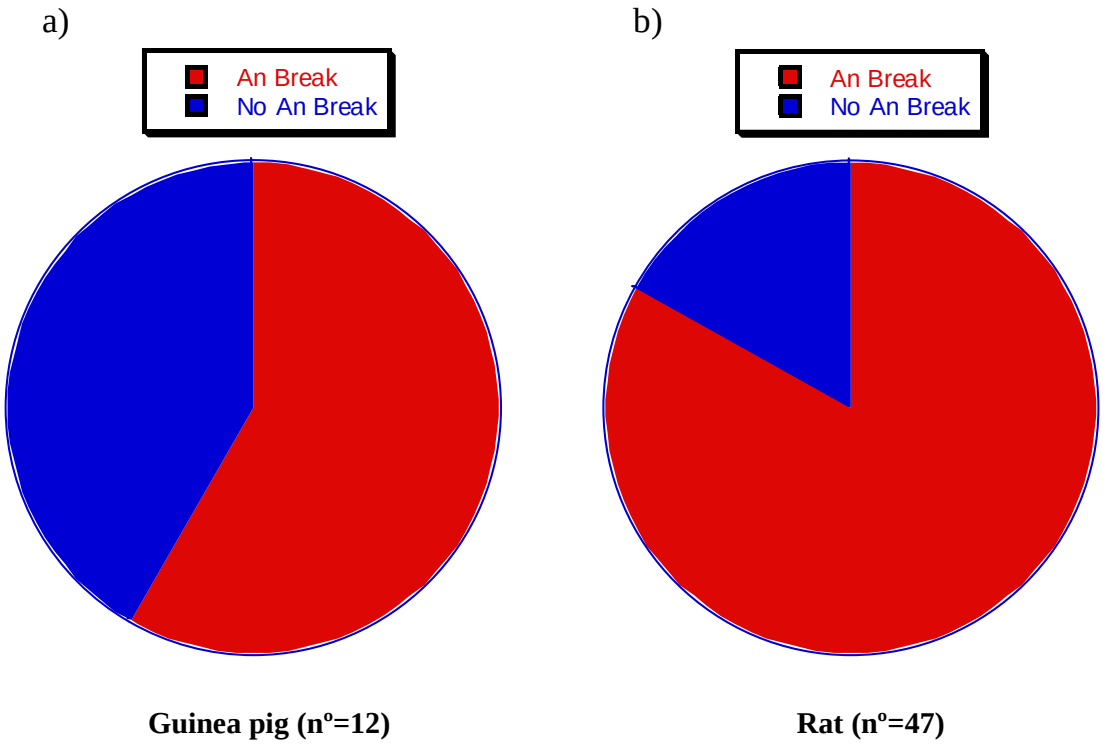

Figure 2. Likelihood of eliciting anode-break action potentials in guinea pig and rat.

a) 7 of 12 (58.3%) guinea pig and b) 39 of 47 (82.9%) rat ventricular cardiomyocytes exhibit anode break excitation.

“Strength-duration” curves and characteristics of anode break action potentials

Strength-duration curves, as a global index of excitability, for guinea pig and rat ventricular cardiomyocytes undergoing electrical stimulations with depolarizing (cathode make) and hyperpolarizing (anode break) current pulses were measured and compared (figure 3). Mean rheobase for cathode make was 0.62 nA for guinea pig and 0.73 nA for rat, whereas mean rheobase for anode break was increased both in guinea pig 16.5 nA and rat 13 nA. We found that the ratio between anodal and cathodal rheobases was much higher in guinea pig than in rat: 26,6 vs 17,8, which are in agreement with the results shown in figure 2. In fact more this ratio is high more current is necessary in order to have anode break excitation and so the anodal threshold is higher in guinea pig than rat.

We also found that maximum rate of depolarization (dV/dt_{max}) increased during anode break as compared with cathodal stimulation and did more so in rat than in guinea pig (+40% vs +13%). Mean dV/dt_{max} for cathode make was 258.5 V/S for guinea pig and 95.3 V/S for rat, whereas mean dV/dt_{max} for anode break was 291.5 V/S for guinea pig and 159.6 V/S for rat (figure 5). It is evident that mean anodal dV/dt_{max} is higher both in guinea pig and rat. In rat this difference was significant. Contemporary action potential models (Beeler and Reuter, 1977; Luo and Rudy, 1994), based on experimental results (Beeler and Reuter, 1970), assume very little steady-state inactivation of the sodium current at the resting potential (e.g., the Luo-Rudy model uses $h = 0.98$ at a resting transmembrane potential of -85 mV, where $h = 1.0$ represents no inactivation and $h = 0$ represents complete inactivation). This observation excludes that an hyperpolarizing stimulus can remove a residual steady state inactivation of the sodium at the resting potential. The decreased cathodal maximum rates of depolarization as compared with anodal that we measured both in guinea pig and rat (significant differences were measured in rat) suggests the existence of a possible degree of residual inactivation of the sodium at the resting potential. The enhanced sodium current upon release of the hyperpolarizing pulse results in a increased anodal dV/dt_{max} as compared with cathodal stimulation. In the figures 6 and 7 examples of action potentials and their dV/dt_{max} elicited by cathode make and anode break stimulation are shown both for guinea pig and rat.

When hyperpolarizing current pulses were consecutively delivered (1Hz) at a fixed duration (3ms) and very close to the current threshold for excitation, action potentials (in rat) were elicited at variable delays after anode break. We found that, in such sequences, action potential amplitude (APA) and dV/dt_{max} decreased linearly with time delay from anode break. Residual steady state inactivation of sodium current at resting potential removed during the hyperpolarizing stimulus is probably recovered in a progressively increasing way during the period of depolarizzaton which precedes the reaching of the sodium threshold (figure 8).

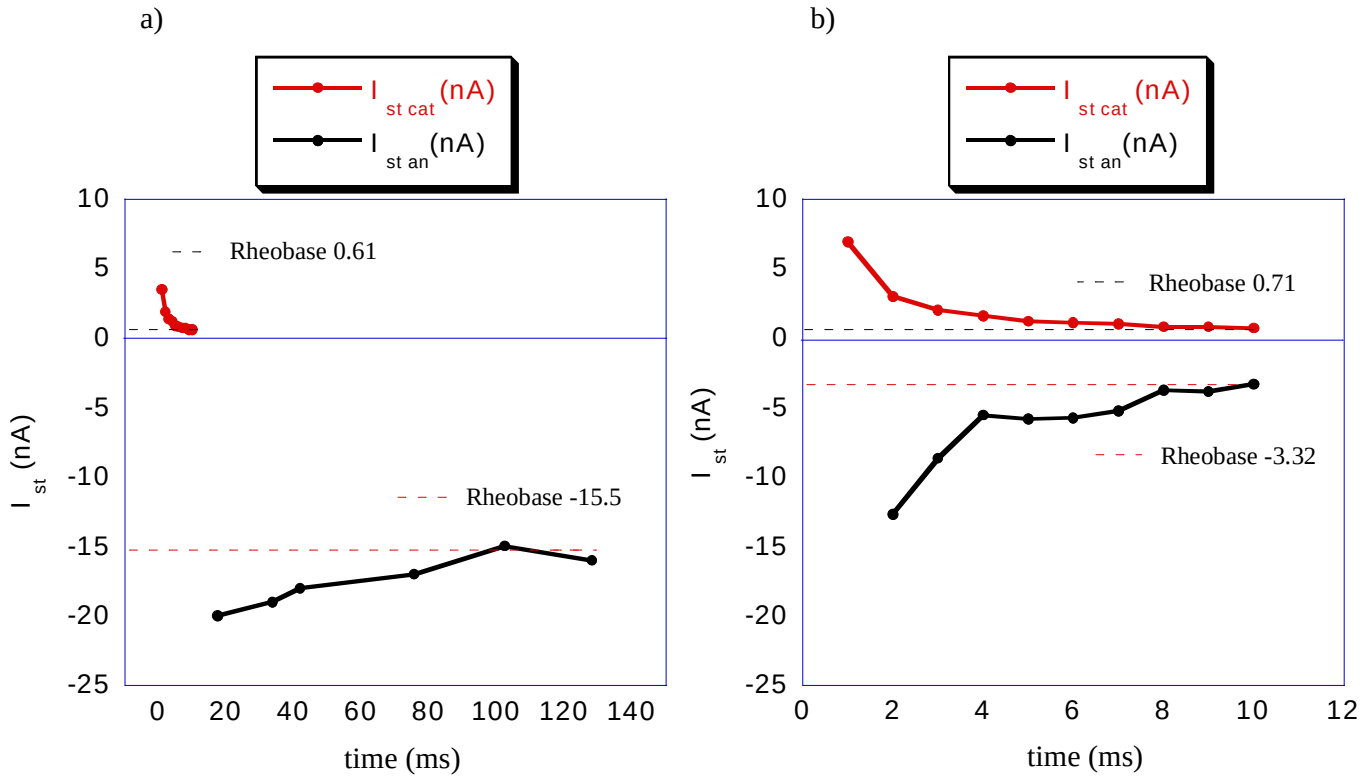

Figure 3. Examples of strength-duration curves for guinea pig a) and rat b). *Cathodal strength durations are plotted in red while anodal strength durations are plotted in black . Note different duration scales on the abscissas between a) and b).*

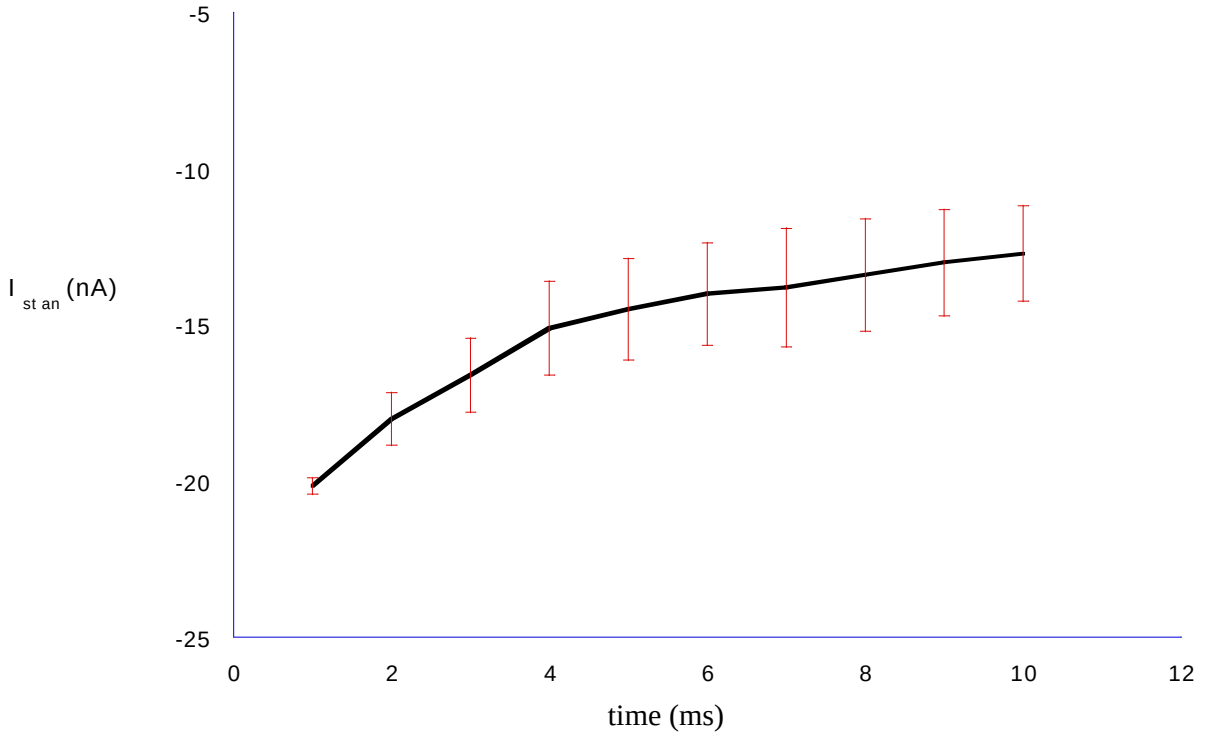

Figure 4. Mean anodal strength-duration curve in rat. *The averages of all current thresholds for each duration of the stimulus (from 1 ms to 10 ms ± S.D.) were measured (nº of "strength-duration" measured = 25).*

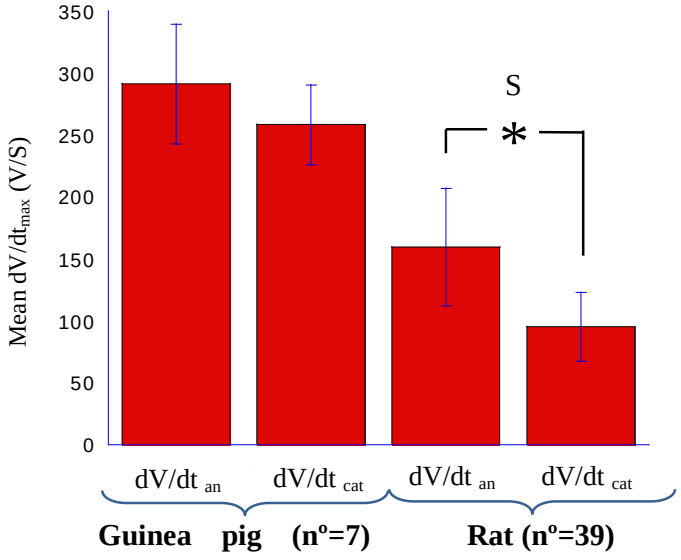

Figure 5. Histograms of the anodal and cathodal dV/dt$_{max}$ mean values. *Anodal dV/dt$_{max}$ was of 291.5 V/S in guinea pig and 159.6 V/S in rat, cathodal dV/dt$_{max}$ was of 258.5 V/S in guinea pig and 95.3 V/S in rat. (* t-test, P<0.1). S: signicative.*

Anode break **Guinea pig ventrcular myocytes** Cathode make

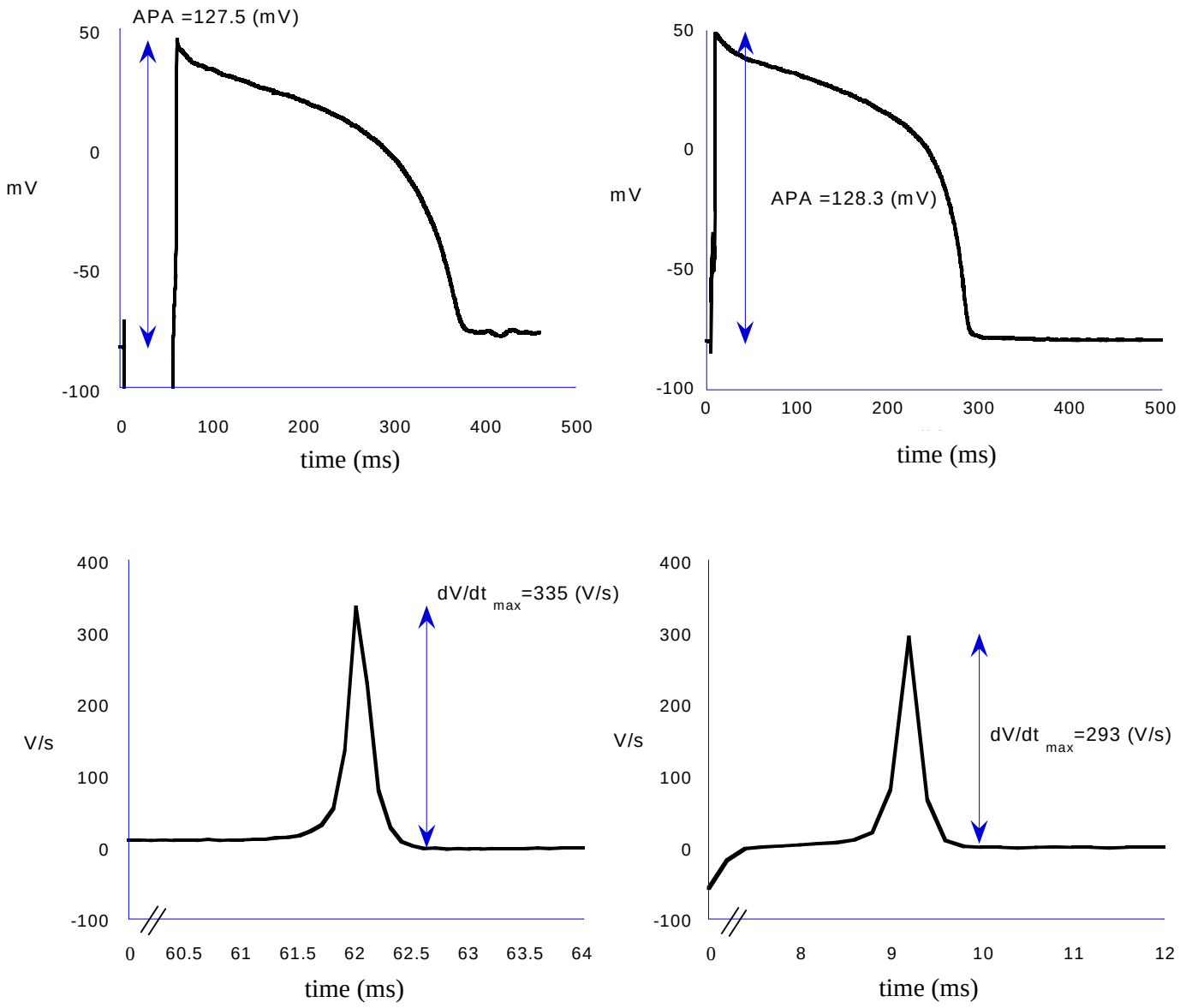

Figure 6. Anodal (on the left) and cathodal (on the rigth) guinea pig action potentials. *APA (above) and dV/dt_{max} (bottom) are compared.*

Anode break **Rat ventricular myocytes** Cathode make

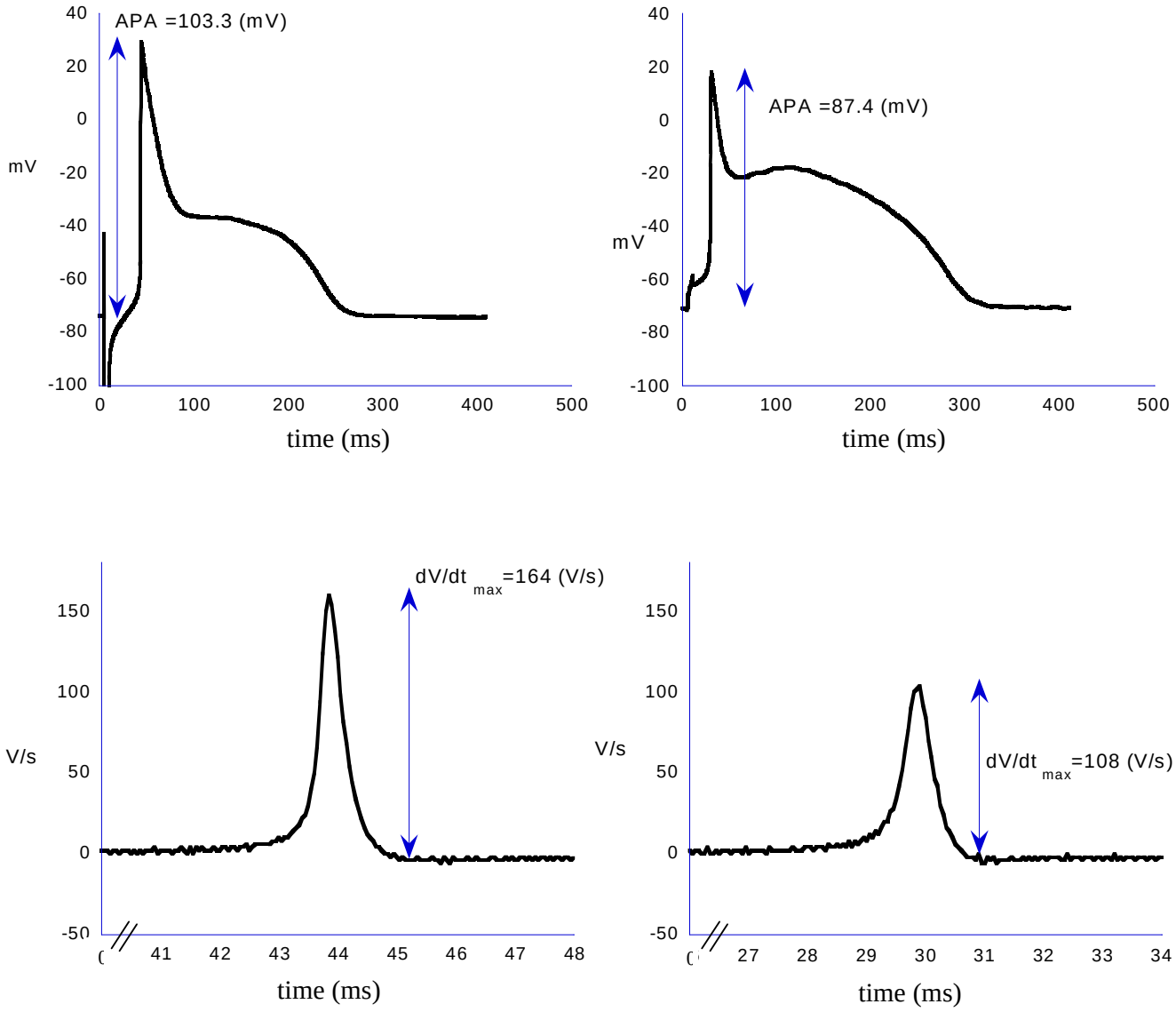

Figure 7. Anodal (on the left) and cathodal (on the rigth) rat action potentials. *APA (above) and dV/dt_{max} (bottom) are compared.*

a)

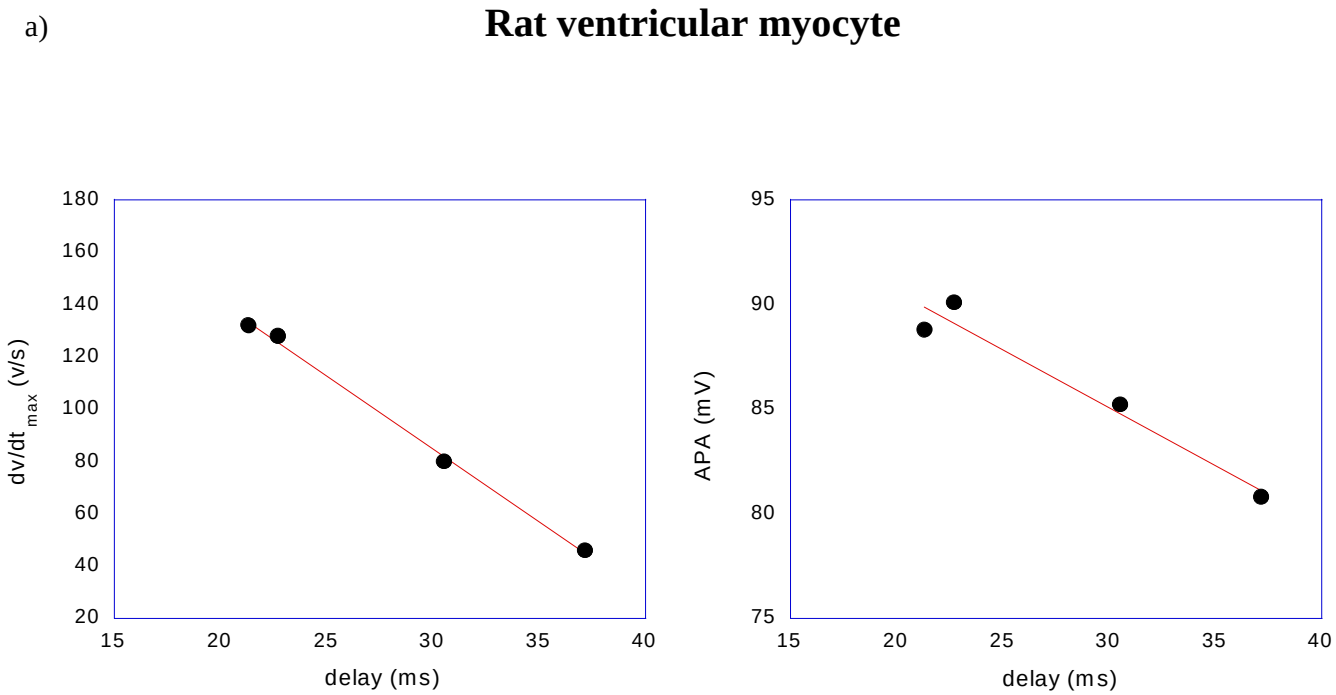

b)

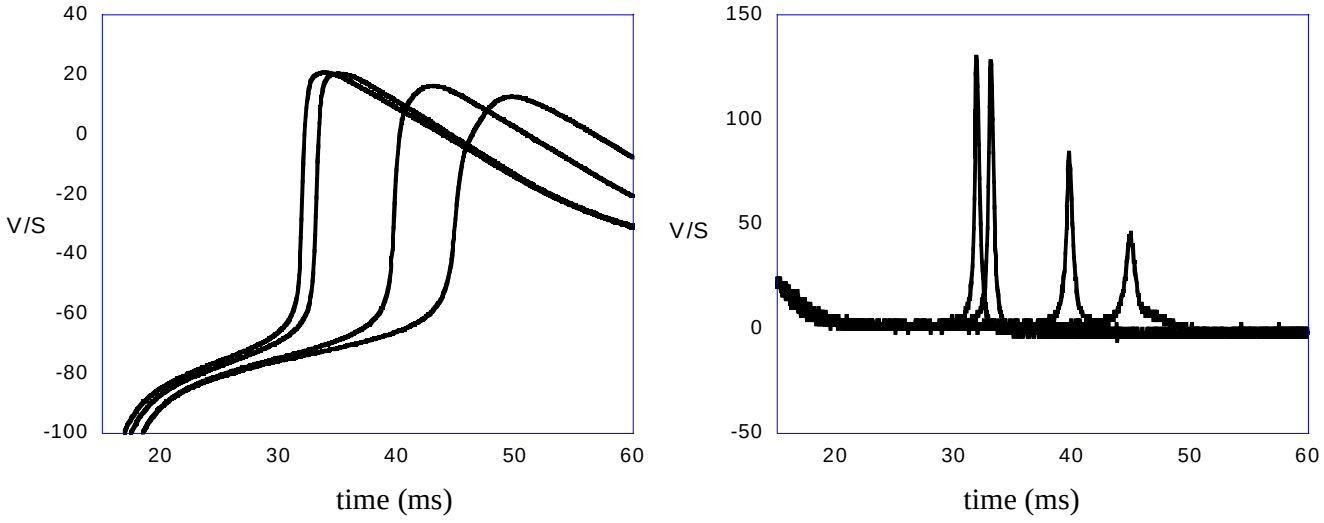

Figure 8. Example of relations between APA and dV/dt$_{max}$. *Above: APA and dV/dt$_{max}$ are plotted as a function of the time delays from action potentials eliciting. Bottom: APA and dV/dt$_{max}$ are plotted as a function of the time. In both relations, APA and dV/dt$_{max}$ decrease linearly with time delay from anode break*

“Supernormal excitability”

The existence of an increase of the excitability in the refractory heart to anode break excitation as compared with its diastolic values was demonstrated by Dekker (Dekker, 1970). Dekker studied thresholds to anodal make, anodal break, cathodal make and cathodal break throughout the cardiac cycle in 13 dogs. Unipolar direct current pulses were applied through epicardial pacemaker electrodes to the left ventricle. Make and break responses were separated by letting the break and make occur in the refractory periods of the following and preceding cycle, respectively. It was found that the left ventricle of the dog could be excited by direct current in all four modes: cathodal make, cathodal break, anodal make, and anodal break. Each of these excitation modes was found to have a different threshold interval curve. The anodal break and cathodal break curves showed an early diastolic “dip”. “Dip” were deepest in the anodal break curves. These had also the shortest effective refractory period (figure 9).

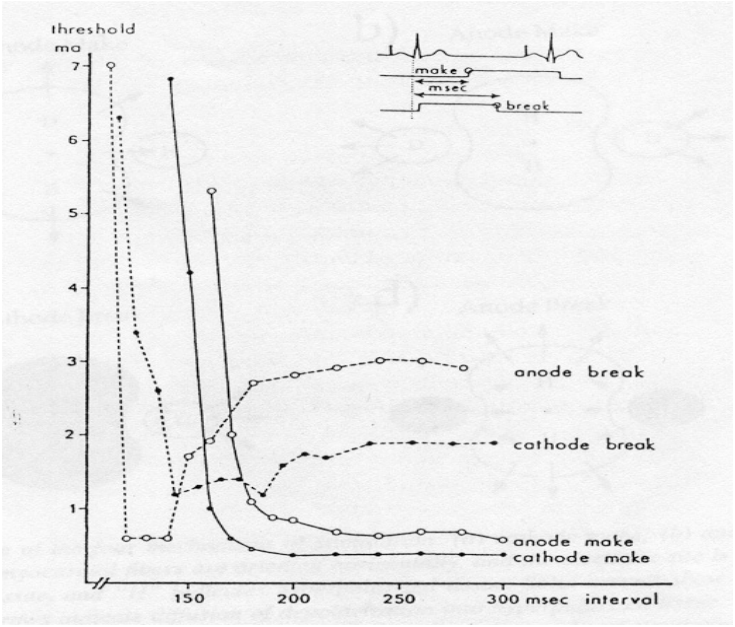

Figure 9. “Strength-intervals” curves in canine ventricle. *Myocardial thresholds in milliamperes are plotted as a function of the interval in milliseconds after the preceding normally conducted QRS complex for each mode of stimulation: anodal make, anodal break, cathodal make and cathodal break. (From Dekker, 1970).*

Anodal stimulation of cardiac tissue has been explained using bidomain models of cardiac tissue relying solely on passive cardiac tissue properties. Bidomain models postulate different electrical anisotropies in the intracellular and interstitial domains of the heart and that the unequal anisotropy in the two domains will lead to marked inhomogeneties membrane potential in nearby tissue (Roth and Wikswo, 1994). Bidoman model predicts excitation to occur at the "virtual cathodes" induced in response to anodal stimulation. These virtual cathodes are predicted to be induced a few millimeters from the stimulating electrode. For anode break stimulation, the bidomain model assumes that a steady state has been reached during the anodal pulse with regions of hyperpolarized and depolarized tissue; upon termination of the stimulus pulse, excitation propagates from the hyperpolarized tissue region as a result of depolarization diffusing from the virtual cathode which is set up solely due to passive tissue properties. Also "supernormal excitability" to anode break, as defined by Dekker, has been attributed to the unequal anisotropy existing in intracellular and extracellular domains and so to a mechanism that is independent from the excitability at cellular level. "Strength-interval" curves that are shown in figure 10 prove, for the first time, that supernormal excitability of the refractory heart to anode break excitation has its source at the cellular level.

When approaching refractory period anodal stimulations showed a temporary threshold increase which then decreased in a typical minimum value (Dekker observed this value in the tissue, "dip") that was lower than diastolic thresholds (region of "supernormal excitability" indicated in figures with arrows).

The curves reported in the figures below show the existence of a mecchanism of "supernormal excitability" to anode break intrinsic at cellular level.

Anodal "strength-interval" curves in rat ventricular myocytes

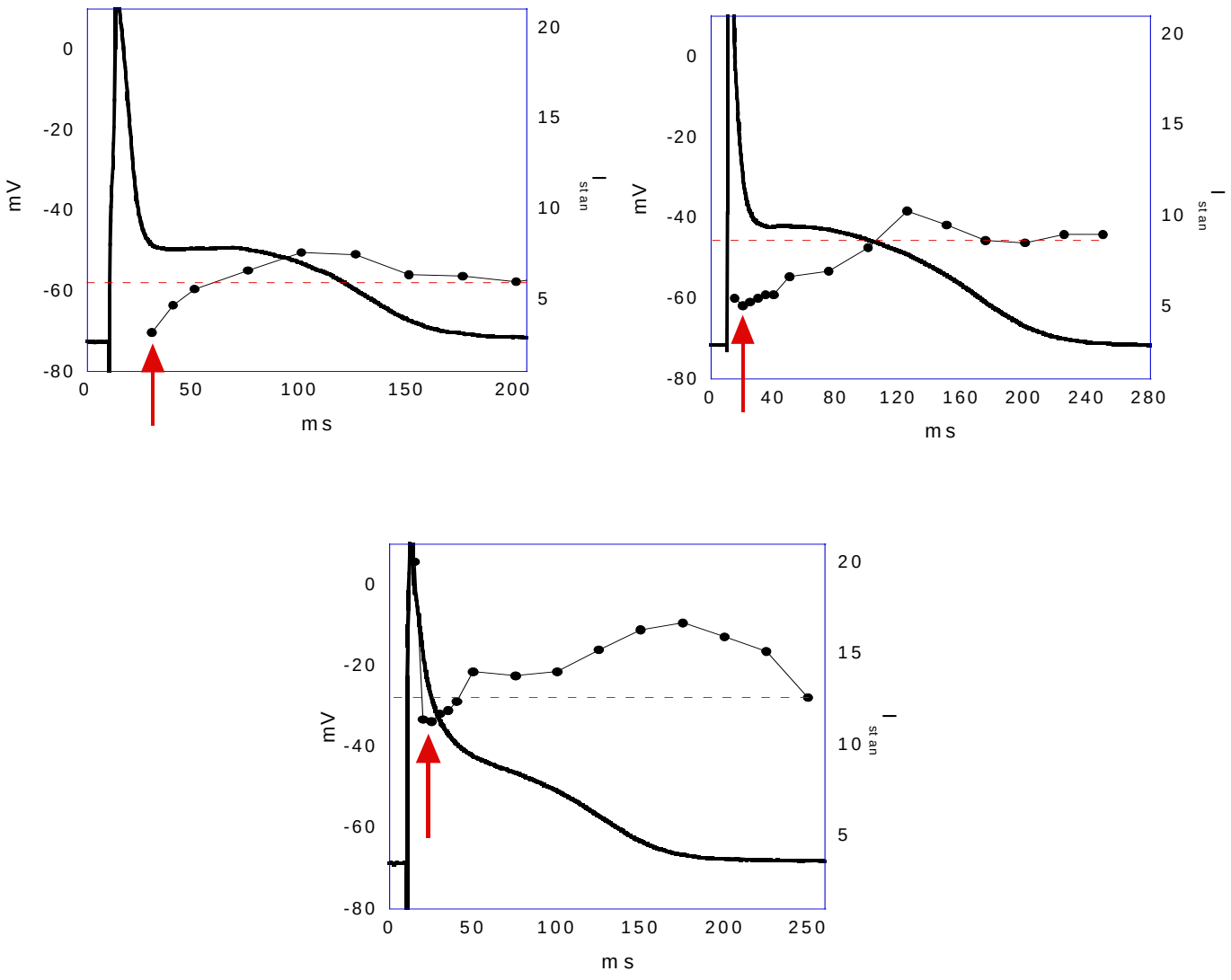

Figure 10. Anodal "strength-interval" curves. *Curves are plotted in function of the corresponding fifth conditioning action potential. Current thresholds (on the right) are plotted as a function of the interval. APA is plotted on the left . Dashed lines divide the curves in parts where there are temporary increases of thresholds and parts of "Supernormal excitability". Arrows indicate the "Supernormal excitability" parts of the curves.*

Cathodal “strength-interval” curves in rat ventricular myocytes

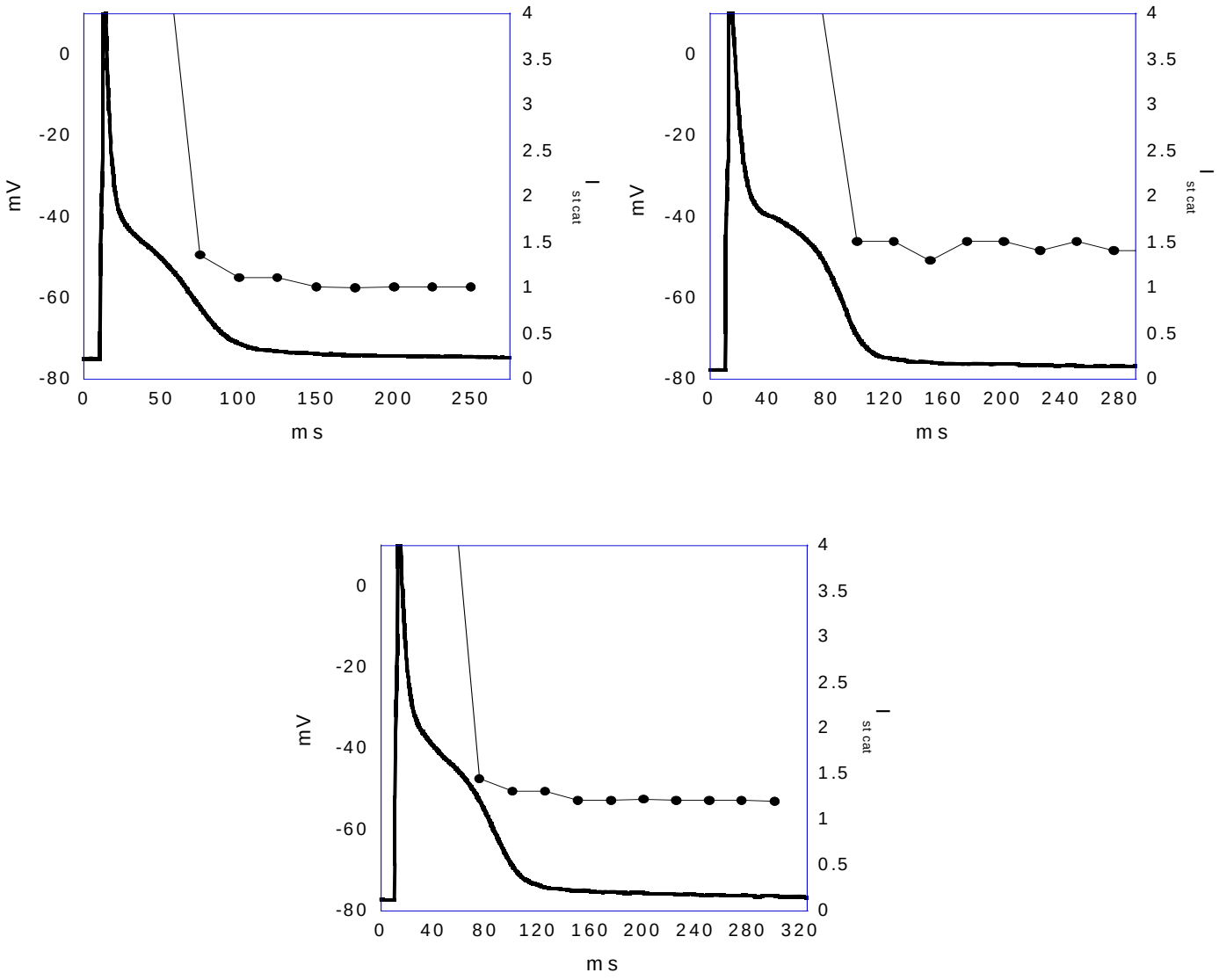

Figure 11. Cathodal “strength-interval” curves. *Curves are plotted in function of the corresponding fifth conditioning action potential. Current thresholds (on the right) are plotted as a function of the interval. APA is plotted on the left .*

Conclusions and future developments

The aim of this work was to define characteristics and properties of the anode break excitation in single guinea pig and rat ventricular cardiomyocytes. We have proved that: 1) anode break excitation is consistent at cellular level, 2) anode break excitation is different in guinea pig and rat ventricular myocytes, 3) the anodal threshold is higher in guinea pig than in rat ventricular myocytes (more current is necessary in order to have anode break excitation), 4) differences in characteristics of anodal and cathodal action potentials (APA and dV/dt_{max}) measured both in guinea pig and rat ventricular myocytes suggest the existence of residual inactivation of the sodium at resting potential of the two species, 5) the phenomenon of "supernormal excitability", which was been observed only in the tissue, is intrinsic to the mechanism of cellular excitability (the anodal "strength-interval" curve in single rat ventricular myocytes was measured for the first time in this research).

These findings are important for the possibility to use the anodal stimulation in a pacemaker programmed to bipolar pacing configuration. Permanent cardiac pacing is the standard treatment for a variety of symptomatic bradycardias. Modern pacemakers can often be programmed either to unipolar or bipolar pacing and/or sensing configurations, allowing the use of either unipolar or bipolar leads. In unipolar configuration, the electrode stimulating the cardiac chamber, typically the cathode (negative pole) of the pacing circuit, must be in direct contact with the myocardium, whereas the other pole completing the electric circuit, the anode, is provided by an electrode not in contact with heart muscle, typically the pacemaker can. In bipolar configuration, both the anode and the cathode are in contact with the heart. For example, in order to increase intraventricular synchronization, especially in the presence of a dilated or ischemic cardiomyopathy, dual site activation of the left ventricle could be achieved by bipolar lead capable of both cathodal and anodal capture. However, anodal pulses might imply a higher arrhythmic risk than cathodal pulses, due to a lower threshold in the refractory period. The absolute refractory period is typically shorter after anodal than cathodal stimulation. Consequently, if a stimulus falls in the vulnerable period of a spontaneous cycle, the risk of triggering a tachyarrhythmia is higher with anodal than cathodal stimulation (Merx et al., 1975). The understanding of

the cellular mechanism of the supernormal anodal excitability during the repolarization phase of action potentials open the possibility to use a pacemaker in the bipolar pacing configuration ensuring anodal stimulation safety.

References

Beeler, G. W., Jr., and H. Reuter. 1970. Voltage clamp experiments on ventricular myocardial fibres. *J. Physiol. (Lond).* 207:165-1

Biermans, G., J. Vereecke, and E. Carmeliet. 1989. Effect of external K on the block of the inward rectifier during hyperpolarization in guinea-pig ventricular myocytes by external Na. *Biomed. Biochim. Acta.* 48:S358-S363

Brooks, C. M., B. F. Hoffman, and E. E. Suckling. 1955. Excitability of the Heart. Grune and Stratton, New York. 82-123.

Carmeliet, E. 1980. Decrease of K efflux and influx by external Cs ions in cardiac Purkinje and muscle cells. *Pflugers Arch.* 383:143-150

Cerbai, E., M. Barbieri, and A. Mugelli. 1994. Characterization of the hyperpolarization-activated current, *I*(*f*), in ventricular myocytes isolated from hypertensive rats. *J. Physiol. (Lond.).* 481:585-591

Cerbai, E., M. Barbieri, and A. Mugelli. 1996. Occurrence and properties of the hyperpolarization-activated current If in ventricular myocytes from normotensive and hypertensive rats during aging. *Circulation.* 94:1674-1681

Cerbai, E., R. Pino, F. Porciatti, G. Sani, M. Toscano, M. Maccherini, G. Giunti, and A. Mugelli. 1997. Characterization of the hyperpolarization-activated current, If, in ventricular myocytes from human failing heart. *Circ.* 95:568-571

Cranefield, P. F., B. F. Hoffman, and A. A. Siebens. 1957. Anodal excitation of cardiac muscle. *Am. J. Physiol.* 190:383-390.

Dekker, E. 1970. Direct current make and break thresholds for pacemaker electrodes on the canine ventricle. *Circ. Res.* 27:811-823

Furman, S., D. L. Hayes, and D. R. Holmes. 1989. A Practice of Cardiac Pacing. Futura Publishing Co., Mount Kisco, NY. 39-42.

Henriquez, C. S., N. Trayanova, and R. Plonsey. 1990. A planar slab bidomain model for cardiac tissue. *Ann. Biomed Eng.* 18:367-376

Henriquez, C. S. 1993. Simulating the electrical behavior of cardiac tissue using the bidomain model. *Crit. Rev. Biomed. Eng.* 21:1-77

Hoffman, B. F., and P. F. Cranefield. 1960. Electrophysiology of the Heart. McGraw-Hill, New York. 211-233.

Luo, C. H., and Y. Rudy. 1994. A dynamic model of the cardiac ventricular action potential. I. Simulations of ionic currents and concentration changes. *Circ Res.* 74:1071-1096

Mitra, R. L., and M. Morad. 1991. Permeance of Cs^+ and Rb^+ through the inwardly rectifying K^+ channel in guinea pig ventricular myocytes. *J. Membr. Biol.* 122:33-42

Roth, B. J. 1992. How the anisotropy of the intracellular and extracellular conductivities influences stimulation of cardiac muscle. *J. Math Biol.* 30:633-64

Roth, B. J. 1995. A mathematical model of make and break electrical stimulation of cardiac tissue by a unipolar anode or cathode. *IEEE Trans. Biomed. Eng.* 42:1174-1184

Roth, B. J. 1994. Mechanisms for electrical stimulation of excitable tissue. *Crit. Rev. Biomed. Eng.* 22:253-305

Roth, B. J. 1996. Strength-interval curves for cardiac tissue predicted using the bidomain model. *J. Cardiovasc. Electrophysiol.* 77:722-737.

Wikswo, J. P., Jr. 1994. The complexities of cardiac cables: virtual electrode effects. *Biophys. J.* 66:551-553.

Wikswo, J. P., Jr., S. F. Lin, and R. A. Abbas. 1995. Virtual electrodes in cardiac tissue: a common mechanism for anodal and cathodal stimulation. *Biophys. J.* 69:2195-2210

Yu, H., F. Chang, and I. S. Cohen. 1993. Pacemaker current exists in ventricular myocytes. *Circ Res.* 72:232-236.

Yu, H., F. Chang, and I. S. Cohen. 1995. Pacemaker current *i*(*f*) in adult canine cardiac ventricular myocytes. *J. Physiol. (Lond.).* 485:469-483.